Dual-windowed Vision Transformer with Angular Self-Attention

Weili Shi   *rhs2rr@virginia.edu*
School of Data Science
University of Virginia

Sheng Li   *shengli@virginia.edu*
School of Data Science
University of Virginia

Reviewed on OpenReview: *https://openreview.net/forum?id=7jgu4oXsGM*

Abstract

Following the great success in natural language processing, transformer-based models have emerged as the competitive model against the convolutional neural networks in computer vision. Vision transformer (ViT) and its subsequent variants have exhibited promising performance in tasks such as image classification, object detection and semantic segmentation. The core of vision transformers is the self-attention mechanism, which models the long-range dependency of different tokens. Conventionally, the attention matrix in self-attention is calculated by the scaled dot-product of *query* (Q) and *key* (K). In this case, the attention weight would depend on the norm of Q and K as well as the angle between them. In this paper, we propose a new attention mechanism named angular self-attention, which replaces the scaled dot-product operation with the angular function in order to effectively model the relationship between tokens. In particular, we propose two forms of functions: quadratic and cosine functions, for our angular self-attention. Based on angular self-attention, we design a new vision transformer architecture called dual-windowed angular vision transformer (**DWAViT**). DWAViT is a hierarchical-structured model characterized by the angular self-attention and a new local window mechanism. We evaluate DWAViT on multiple computer vision benchmarks, including image classification on ImageNet-1K, object detection on COCO, and semantic segmentation on ADE20K. Our experimental results also suggest that our model can achieve promising performance on the tasks while maintaining comparable computational cost with that of the baseline models (e.g., Swin Transformer). The source code is available at `https://github.com/DamoSWL/DWAViT`.

1 Introduction

Vision transformers have received tremendous attention since its emergence. Inspired by the success of the transformer (Vaswani et al., 2017) in the sequence modeling, Dosovitskiy et al. (Dosovitskiy et al., 2021) proposed the initial architecture of vision transformer which can be regarded as the encoder part of the original transformer (Vaswani et al., 2017). Compared to convolutional neural networks (CNNs), the vision transformer is featured by its ability to transform the spatial visual representation learning on the image into the token-to-token learning, by partitioning the image into multiple patches. Benefited from the ability of the self-attention mechanism that can model the long-range dependence of tokens in the image, vision transformers exhibit on par or better performance against CNNs in many computer vision tasks Shi et al. (2022; 2023); Zhou et al. (2022b); Chen et al. (2023a); Wang et al. (2023a;b), such as image classification (Dosovitskiy et al., 2021; Dong et al., 2022), object detection (Carion et al., 2020; He & Todorovic, 2022; Zhang et al., 2022a), and semantic segmentation (Zheng et al., 2021; Xie et al., 2021). Despite the merits mentioned above, the shortcoming of vision transformer is also obvious. The low level of the inductive bias requires more large

datasets such as Image-21K (Deng et al., 2009) and JFT300M (Sun et al., 2017) for model training. Besides, the time complexity of the self-attention computation is quadratic to the number of input tokens, which prohibits the application of vision transformers on the tasks that basically involve high-resolution images.

To deal with the excessive computation of the self-attention, the subsequent work (Liu et al., 2021; Dong et al., 2022; Huang et al., 2019; Wang et al., 2020; Xia et al., 2022) proposed different local-window mechanisms to restrict the computation of self-attention in a local window. For instance, the pioneering work Swin Transformer (Liu et al., 2021) adopts the shift windows to reduce the workload of computing self-attention and to facilitate the interaction of local windows. CSwin (Dong et al., 2022) proposes the cross-shaped window, in which the image is split into the horizontal and vertical strips in parallel. Another work (Xia et al., 2022) presents a flexible local window, which could be implemented in a data-dependent way.

Another branch of work (Qin et al.; Katharopoulos et al., 2020; Peng et al.; Choromanski et al.) focuses on the in-depth understanding of the self-attention mechanism and proposes new formulations to calculate the attention scores between different pairs of tokens. From the perspective of kernel learning, the interaction of the query and key can be modeled by specific kernel function, and the scaled dot-product operation can be replaced by the softmax-free operation in self-attention. Usually, the softmax-free operation can lower the time complexity of the computation in self-attention.

In this paper, we present new designs on the local window mechanism and the operation in self-attention. In terms of the local window, we propose a dual window mechanism. As shown in Fig. 1, similar to Swin Transformer (Liu et al., 2021), the local window is also imposed on the feature maps for the purpose of reduction of the time complexity. However, unlike
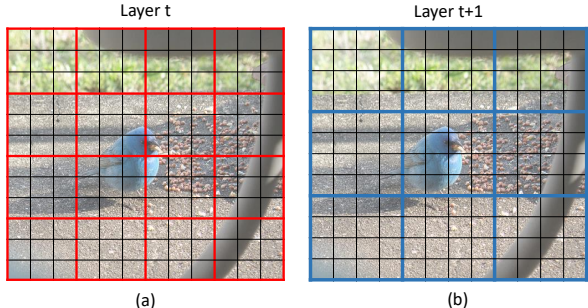

Figure 1: The illustration of the dual window mechanism. The image is partitioned into (a) even number of local windows and (b) odd number of local windows in two layers, respectively. The size of the local window is flexible and the tokens lie on the border of one local window would reside in the interior of the local window in the following layer. The connection of the local window in each layer can be bridged by the operation of the local window in the next layer.

the previous work in which the size of the local window is fixed, the size of our proposed local window is flexible and is adjustable according to the size of the feature maps. Besides, to mitigate the problem of lacking connections between local windows, the number of local windows is different at layer t and layer $t + 1$. For instance, there are even numbers of the local windows at layer t but odd numbers of local windows at layer $t + 1$. In this case, the tokens that lie in one local window from the first feature map would belong to another local window in the following features map. Since the feature maps are partitioned into different numbers of local windows, the coordinates of the local windows in the adjacent feature maps are different. The tokens in the overlapping area of local windows can bridge the connection of local windows since these tokens would participate in the self-attention calculation within each local window. With the interaction of the local windows, receptive fields can be enlarged implicitly, and the ability to model long range relations can also be enhanced considerably.

In traditional self-attention mechanism, the similarity of the query and key is computed by the scaled dot-product. Thus, the similarity would depend on the norm of query and key as well as the angle between them. Inspired by previous work (Wang et al., 2018; Zhao et al., 2020), we notice that scaled dot-product function is not the only choice to model the relationship of tokens. In this paper, we propose the angular self-attention, in which the similarity of query and key is only dependent on the angle between them. To reduce the impact of the norm of the query and key on the relation of tokens, the query and key are L2-normalized, and query and key are distributed on the unit sphere. The relationship of the query and key would be determined by the angle between them, and a smaller angle could yield a larger attention score between a pair of query and key. In angular self-attention, we adopt two forms of functions: quadratic and cosine functions, to model this relationship, and the similarity is further enlarged by the temperature scaling. Besides, we also propose a new linear function to simplify the computation in the quadratic self-attention. Our experiments show that the angular self-attention can serve as the alternative for the traditional scaled dot-product self-attention.

Jointly combining the dual window mechanism and angular self-attention, we propose a novel hierarchical-structured vision transformer backbone called dual-windowed angular vision transformer (DWAViT). In DWAViT, the attention score for each pair of query and key is modeled by the temperature-scaled quadratic/cosine functions, and experimental results validate that our quadratic/cosine functions are effective in modeling the relationship between tokens. Besides, the dual window mechanism is also adopted in our new backbone. The feature maps are partitioned into even/odd numbers of local windows in the layers of DWAViT alternatively. The dual window mechanism can preserve the ability to model long-range relationships between tokens. With proper partition of the feature maps, our DWAViT can be applied to the downstream tasks (e.g., object detection, semantic segmentation) which involve high-resolution images and achieve comparable computational cost with that of baseline models (i.e., Swin Transformer (Liu et al., 2021)). The major contributions of this paper are as follows:

- We propose the dual window mechanism to split the global feature map into a couple of smaller localized feature maps. By partitioning the feature maps in even/odd numbers of local windows in an alternative way, the lack of connection between local windows can be alleviated.

- We propose the angular self-attention in which the scaled dot-product operation is replaced by the temperature-scaled quadratic/cosine functions. A linear function is also proposed to simplify the computation in quadratic self-attention. Our proposed angular self-attention can model the long range relationship of tokens and is the competitive alternative for the scaled dot-product self-attention.

- The dual-windowed angular vision transformer (DWAViT) is proposed by jointly combining the dual window and angular self-attention. The DWAViT is evaluated on a series of dense prediction tasks and achieves competitive performance on ImageNet image classification, COCO object detection, and ADE20K semantic segmentation. With proper partition of the local windows, our model can achieve comparable computational cost as that of the baseline models.

2 Related Work

Vision Transformers. The pioneering work (Parmar et al., 2018; Wang et al., 2018) first introduced the self-attention mechanism to the computer vision field and some early work Ramachandran et al. (2019); Cordonnier et al. (2019) applied self-attention in the computer vision tasks. Dosovitskiy et al. (Dosovitskiy et al., 2021) proposed the transformer-based backbone architecture called vision transformers (ViTs) (Dosovitskiy et al., 2021). With the new paradigm of representative learning, ViTs achieve on par or better performance on image classification, object detection and semantic segmentation against CNNs. Since the emergence of vision transformers, plenty of work (Touvron et al., 2021a; 2022) has been done on this field and the subsequent work aims to improve the ViTs on different aspects. DeiT (Touvron et al., 2021a; 2022) proposes new training recipe to reduce the high demand of ViTs for the very large datasets. With the techniques provided by DeiT (Touvron et al., 2021a; 2022), ViTs can pretrained from scratch on smaller datasets such as ImageNet-1K (Deng et al., 2009) compared to ImageNet-21K (Deng et al., 2009) and JFT300M (Sun et al., 2017). Besides, ViTs also borrow the idea form the modern CNN architectures (Wang et al., 2023c; He et al., 2016; Howard et al., 2017; Sandler et al., 2018; Tan & Le, 2019; 2021; 2019; Huang et al., 2017; Liu et al., 2022b; Rao et al.; Wang et al., 2022a; Dai et al., 2021) to improve the ability of representative learning and develop hierarchical pyramid structure to handle the multi-scale feature maps. The pyramid-structured ViTs usually have four stage and in each stage the size of the feature maps is half of that in the previous stage while the dimension is doubled. Another line of work (Wu et al., 2021; Guo et al., 2022; Xiao et al., 2021; Tu et al., 2022; Yuan et al., 2021; Srinivas et al., 2021; Chen et al., 2022; Mehta & Rastegari; Peng et al., 2021) incorporates the convolution operation into the architecture of the vision transformers at different location. The performance of the hybrid vision transformers are further improved by fusing the local information learned by CNNs and global dependence information obtained by self-attention. To mitigate the computational cost of the global self-attention which is quadratic to the size of the input features. Some work (Tian et al., 2023; Lee et al., 2022; Chen et al., 2021) learn the contextual information from the multi-scale patch embedding. An extensive work (Hatamizadeh et al., 2023; Chen et al., 2023b; Hassani et al., 2023; Dong et al., 2022; Liu et al., 2022a; 2021; Xia et al., 2022; Wang et al., 2020; Hassani et al., 2022; Han et al., 2021; Huang et al.,

2019; Ren et al., 2022) proposes different local window mechanism to reduce the computational cost. The self-attention is performed within the local windows and the connection of different local window is achieved by some techniques such as shifted window (Liu et al., 2021) or cross-shaped window (Dong et al., 2022). Another line of work Shi & Li (2022); Zhou et al. (2022a); Mao et al. (2022) suggested that vision transformers exhibit stronger robustness to adversarial attacks that CNNs. In our paper we propose a new local window mechanism called dual window and the connection of local windows can be achieved in a simple way.
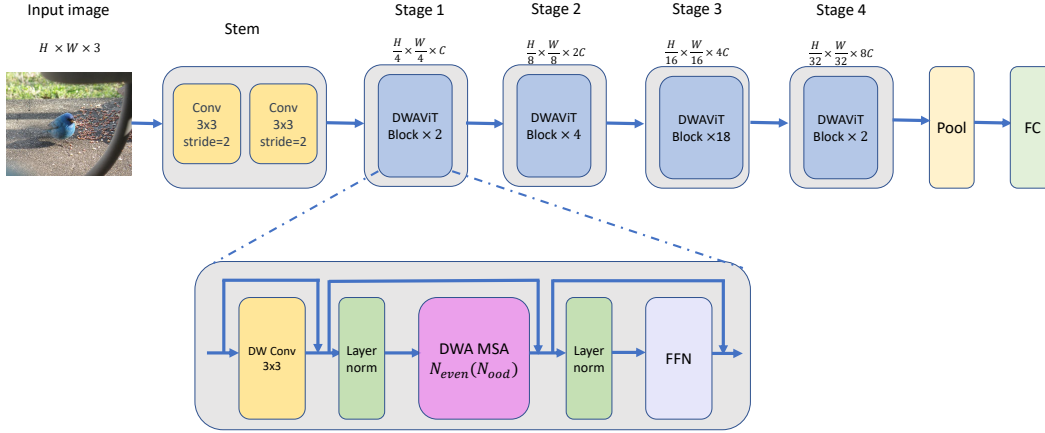

Figure 2: The illustration of our proposed dual-windowed angular vision transformer (DWAViT). Similar to previous work our backbone adopts the hierarchical pyramid structure. The core module in our backbone is the dual-windowed angular multi-head self-attention (DWA MSA) which jointly combines the dual window mechanism and angular self-attention. In each block the feature maps are divided into even/odd numbers of local windows. Besides. The depthwise convolution provides the conditional positional embedding.

Self-attention. Apart from the traditional scaled dot-product self-attention, different forms of self-attention mechanism are also proposed. Early work (Wang et al., 2018; Zhao et al., 2020) explored the general form of the function in the self-attention and proposed several operations such as dot-product and concatenation. XciT (Ali et al., 2021) proposed cross-covariance attention (XCA) in which the attention is performed on g over channels instead of tokens. MaxVit (Tu et al., 2022) and DaViT (Ding et al., 2022) proposed grid attention and channel group attention, respectively. These attentions are also performed on channels dimension rather than spatial dimension. To reduce the the computational cost, the efficient self-attention(Han et al., 2023; Dao et al., 2022; Sun et al., 2023; Katharopoulos et al., 2020) is proposed to approximate the traditional softmax self-attention. Linear transformer (Katharopoulos et al., 2020) suggests that softmax function can be removed and the similarity of tokens can be obtained by pure dot product of query and key. RFA (Peng et al.) and performer (Choromanski et al.) approximate the softmax attention with positive random features. CosFormer (Qin et al.) proposed cos-based re-weighting self-attention in which the attention score is calculated by the weighted dot-product of query and key. In SOFT (Lu et al., 2021), the dot-product similarity is replaced by the Gaussian kernel function. In our paper, we also propose a new self-attention mechanism called angular self-attention, in which the similarity of tokens is calculated from a quadratic function.

3 Methodology

3.1 Dual Window

As shown if Fig. 1, the feature maps is partitioned into even number of local windows and odd number of local windows at layer t and layer t+1 alternatively. The feature maps is padded if necessary. Suppose the original size of feature map is $h \times w$. after the padding, the size of the padded feature map is $h' \times w'$. The number of the local window is $N_{even} = n_{even}^2 (N_{odd} = n_{odd}^2)$. $n_{even}(n_{odd})$ is the number of local window per side. Thus, the size of local window is $\frac{h}{n_{even}} \times \frac{w}{n_{even}} (\frac{h}{n_{odd}} \times \frac{w}{n_{odd}})$. Compared to Swin Transformer (Liu et al., 2021) that bridge the connection of different local windows by complicated techniques such as cycle shifted

local window, we solve this problem in a simple way. Notice that tokens lie on the border of one local window would reside in the interior of the local window in the following layer. Therefore, the tokens on the border of the local window at one layer can participate in the self-attention calculation with the tokens from other local windows in the next layer. The dynamic interaction of the local windows can facilitate the propagation of the information between local windows, The actual size of receptive field would be larger than the size of local window and the ability to model the long-range relationship of tokens would also be enhanced.

3.2 Angular Self-Attention

Self-attention can be regarded as weighted combination of the input sequence, where the weights are determined by the similarities between tokens of the input sequence. We use $\mathcal{O}_i \in \mathcal{R}^d$ to denote the generated embedding of token i from self-attention. Then the general form of self-attention could be written as:

$$\mathcal{O}_i = \sum_j \frac{\mathcal{S}(Q_i, K_j)}{\sum_j \mathcal{S}(Q_i, K_j)} V_j, \tag{1}$$

where $\mathcal{S}(\cdot)$ represents the similarities between Q and K and it has many forms according to the previous work (Wang et al., 2018; Zhao et al., 2020). if $\mathcal{S}(Q_i, K_j) = \exp(Q_i \cdot K_j / \sqrt{d_k})$, Eq. 1 would become the scaled dot-product attention as we commonly see in vision transformers. The formulation of scaled dot-product self-attention in vision transformers is $\text{Attention}(Q, K, V) = \text{Softmax}(\frac{QK^T}{\sqrt{d_k}})V$.

In dot-product self-attention, the attention weight is generated from the scaled dot-product between Q and K. The dot-product of Q_i and K_j can be expanded as $Q_i \cdot K_j = \|Q_i\| \|K_j\| \cos\theta$. It indicates that the similarity would depend on the L2 norm of Q and K as well as their angles θ. In our paper, we propose angular self-attention, in which we use angular function $s(\theta)$ to replace the conventional scaled dot-product operation. Then the self-attention could be reformulated as:

$$\mathcal{O}_i = \sum_j \frac{\exp(s(\theta_{ij})/\tau)}{\sum_j \exp(s(\theta_{ij})/\tau)} V_j, \tag{2}$$

where $\theta_{ij} = \arccos(\hat{Q}_i \cdot \hat{K}_j)$, $\hat{Q}$ and $\hat{K}$ are L2 normalized query and key, respectively. τ is the temperature hyper-parameter that regulates the attention weight of each token.

When Q and K are normalized, they can be distributed on the surface of the unit sphere. Then the attention weight obtained from our angular self-attention is solely dependent on the angle θ. Through our training the angles θ between different Q and K would be adjusted to model the relationship of different tokens and make the vision transformer achieve strong representative ability. Thus, we propose two alternative functions for $s(\theta)$ in Eq. 2. They are cosine function $s(\theta) = \cos(\theta)$ and quadratic function $s(\theta) = 1 - \frac{4\theta^2}{\pi^2}$. In angular self-attention, the similarity of Q and K would solely depend on their angles. The matrix form of angular self-attention could be formulated as:

$$\text{Attention}(Q, K, V) = \text{Softmax}(\frac{\hat{Q}\hat{K}^T}{\tau})V$$
$$\text{Attention}(Q, K, V) = \text{Softmax}(\frac{1 - 4\Theta^2/\pi^2}{\tau})V, \tag{3}$$

where $\Theta = \arccos(\hat{Q}\hat{K}^T)$. $\hat{Q}$ and $\hat{K}$ are L2 normalized query and key, respectively. To simplify the computation of Θ, a linear function $\Theta = -(\frac{\pi}{2} - \tau)\hat{Q}\hat{K}^T + \frac{\pi}{2}$ is proposed to approximate arccos function, where τ is the hyper-parameter that determines the closeness between the linear function and arccos function.

The intuition behind our angular-self attention is straightforward. In scaled dot-product attention the similarity score would be dependent on both the norm of the tokens as well as the angle between them. Our intuition is that the norm of the tokens may have a negative impact on the interaction of the query and key. Thus, In our angular self-attention, we design two angular functions to model the similarity of the tokens and reduce the noisy impact from the norm of the query and key. The extensive experiments show that our angular self-attention can successfully model the relationship of the tokens and achieve promising results on different tasks such as classification, object detection and segmentation.

Table 1: The details of the DWAViT variants.

Models	#Dim	#Blocks	#Heads	#Param(M)	#FLOPs(G)
DWAViT-Tiny	[64,128,256,512]	[2,4,18,2]	[1,2,4,8]	22.7	4.18
DWAViT-Small	[80,160,320,640]	[3,6,21,3]	[1,2,4,8]	44.6	8.22
DWAViT-Base	[96,192,384,768]	[4,8,24,4]	[1,2,4,8]	77.4	14.27

The cosine similarity and quadratic distance has common mathematical properties. Both functions are descending when $\theta \in [0, \pi]$, which means that the tokens with larger angles would have less weaker relationships. Specifically, when $\theta \in [0, \pi/2]$, $\cos \theta \approx 1 - \theta^2/2 \approx 1 - 4\theta^2/\pi^2$, when $\theta \in (\pi/2, \pi]$, $1 - 4\theta^2/\pi^2 < \cos \theta < 0$, which means that tokens with angles larger than $\pi/2$ have weaker relationships in quadratic function than that of in cos function. Our experiments suggest that on most tasks the performance of quadratic and cosine functions is comparable and the difference is very slight.

3.3 Overall Architecture

We replace the traditional scaled dot-product self-attention with our angular self-attention, and integrate the dual window mechanism to build our dual-windowed angular vision transformer (DWAViT). The overall illustration of our DWAViT is illustrated in Fig. 2. Similar to the previous work (Wang et al., 2021; 2022b; Ding et al., 2022; Fan et al., 2021; Li et al., 2022; Liu et al., 2021; 2022a), the DWAViT also adopts the hierarchical pyramid structure that take advantage of the multi-scale resolution of feature maps for the dense prediction task. The size of the input image is $H \times W \times 3$. Instead of adopting the convolutional layer with large kernel, we follow the work (Xiao et al., 2021) and leverage the two stacked convolutional layer as the stem to generate patch embedding. For each convolutional layer, the kernel size is 3×3 and the stride is 2×2. The size of the output from the stem is $\frac{H}{4} \times \frac{W}{4} \times C$.

The DWAViT consists of four stages in which the size of the feature maps is half of that from the previous stage while the dimension is doubled compared to that from the previous stage. Between two adjacent stages we adopt a convolutional layer with kernel size of 2×2 and stride of 2 to downsample the feature maps. Each stage consists of multiple blocks which include the depthwise convolution (Chollet, 2017) that generates the conditional positional embedding (CPE) (Chu et al., 2021b), the dual-windowed angular multi-head self-attention (DWA MSA) and feed-forward network (FFN). Compared to absolute positional embedding (APE) (Vaswani et al., 2017)

Figure 3: The illustration of the pipeline in the dual-windowed angular multi-head self-attention (DWA MSA). The Q, K and V are localized by dividing them into a couple of local windows. The scaled dot-product operation is replaced by the temperature-scaled angular function in the calculation of attention matrix.

that could only provide the positional information for the fixed length of sequence, The CPE can provide flexible positional information adaptive to various length of input sequence that is often seen in the downstream tasks. Relative positional embedding (RPE) (Liu et al., 2021; Shaw et al., 2018) provides the relative positional information within the window. However, since the size of the window is different in each stage, RPE (Liu et al., 2021; Shaw et al., 2018) would not be adopted in our DWAViT.
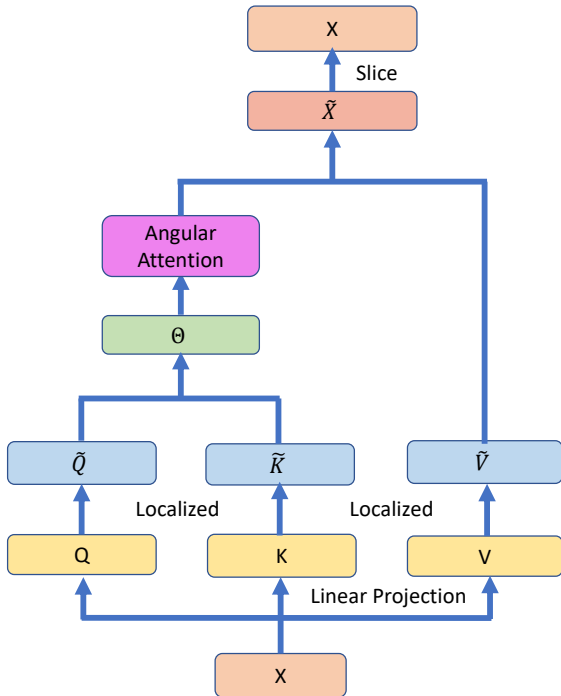
The dual-windowed angular multi-head self-attention (DWA MSA) serves the core function for our backbone. It jointly combines the dual window mechanism and angular self-attention. The details of DWA MSA is illustrated in Fig. 3, Suppose the input feature is $X \in \mathbb{R}^{h \times w \times D}$, $N = N_{even}$ or N_{odd} is the number of local windows and $n = \sqrt{N}$ is the number of local windows per side. After linear projection, we obtain query, key and value Q, K, $V \in \mathbb{R}^{h \times w \times D}$. Instead of splitting the X into smaller local windows, we split Q and K into N local windows. The size of the local window is $\frac{h'}{n} \times \frac{w'}{n}$. The h' and w' are the height and width of the padded feature maps. In each stage, the partition with even/odd number of windows take turns and the value of $N_{even}(N_{odd})$ vary according to the size of the feature maps. After the partition, for k^{th} head, we obtain the localized query $\tilde{Q}^k = \{Q_i^k, Q_2^k, ..., Q_N^k\}$ and key $\tilde{K}^k = \{K_i^k, K_2^k, ..., K_N^k\}$. the localized query and key are L2 normalized and the angle matrix Θ is calculated from the normalized query and key. Next the new embedding is calculated from the localized query, key and value by Eq. 3. The new feature maps of each local window is obtained by the concatenation of the embedding from each head $\tilde{X}_i = \text{concat}(\tilde{X}_i^1, \tilde{X}_i^2, ..., \tilde{X}_i^K)$. K is the number of heads. We concatenate the feature maps of each local window to form the complete feature map $\tilde{X} = \text{concat}(\tilde{X}_1, \tilde{X}_2, ..., \tilde{X}_N)$. The size of $\tilde{X}$ is larger than that of the original feature map. To restore it, the final feature map is obtained from $\tilde{X}$ with slice operation:

$$X = \tilde{X}[\text{top} : h - \text{bottom}, \text{left} : w - \text{right}], \tag{4}$$

where top, bottom, left and right are the size of padding on the top, bottom, left and right of the feature maps, respectively. With all the components aforementioned above, the pipeline of the block in our DWAViT can be formulated as:

$$\begin{aligned} Z^\ell &= \text{DWConv}(X^{\ell-1}) + X^{\ell-1}, \\ \tilde{X}_\ell &= \text{DWA-attention}(\text{LN}(Z^\ell)) + Z^\ell, \\ X_\ell &= \text{FFN}(\text{LN}(\tilde{X}_\ell)) + \tilde{X}_\ell, \end{aligned} \tag{5}$$

where $X^{\ell-1}$ denote the output feature from the ℓth block in the backbone.

In our DWAViT, there are strong connections between the two key components: angular self-attention and dual local window mechanism. On one hand, The dual window mechanism can confine the operation of self-attention in localized areas. On the other hand, our empirical study suggests that our angular self-attention can achieve better performance with our dual local window techniques than that with previous local window techniques (i.e., Swin Transformer (Liu et al., 2021)) for two reasons. First, the partition of the dual local window is implemented on the queries and keys, not on the feature maps directly, which would be helpful for the direct interaction of the tokens. Second, the size of our local window is flexible. And we can choose the optimal window size for tasks with different input resolutions such as object detection and segmentation. To wrap up, the two proposed techniques have strong mutual connections and are two indispensable components.

3.4 Architecture Variants

We build three variants of DWAViT with different numbers of parameters and FLOPs, namely DWAViT-Tiny, DWAViT-Small and DWAViT-Base. For all the variants, the number of local windows in each stage is set to (100,49), (49,16), (4,1), (1,1) in image classification, respectively. In stage one, the size of the local window would be 6×6 and 8×8 in two consecutive blocks. For the downstream tasks such as object detection and semantic segmentation, since the size of the input image is larger, the number of local windows in DWAViT is also different. The details of three DWAViT variants are illustrated in Table 1.

3.5 Time Complexity Analysis

Suppose the original size of the feature map is $h \times w$ and the dimension is C. After padding the size of feature maps becomes $h' \times w'$. The total number of local windows is N. The time complexity of the linear projection is $4hwC^2$. Since the self-attention is performed on the padded feature maps, the time complexity for the self-attention calculation is $2(h'w')^2C/N$. Thus, the total time complexity of our DWA MSA is:

$$\Omega(\text{DWA MSA}) = 4hwC^2 + 2(h'w')^2C/N. \tag{6}$$

As illustrated in Eq. 6, In order to reduce the computational cost, we should choose a large value of N while keeping the h' and w' as close as to the original value. Note that though angular self-attention includes some operations like arccos and L2 normalization, they do not increase the time complexity. However, the memory demand of angular self-attention is larger than that of traditional self-attention.
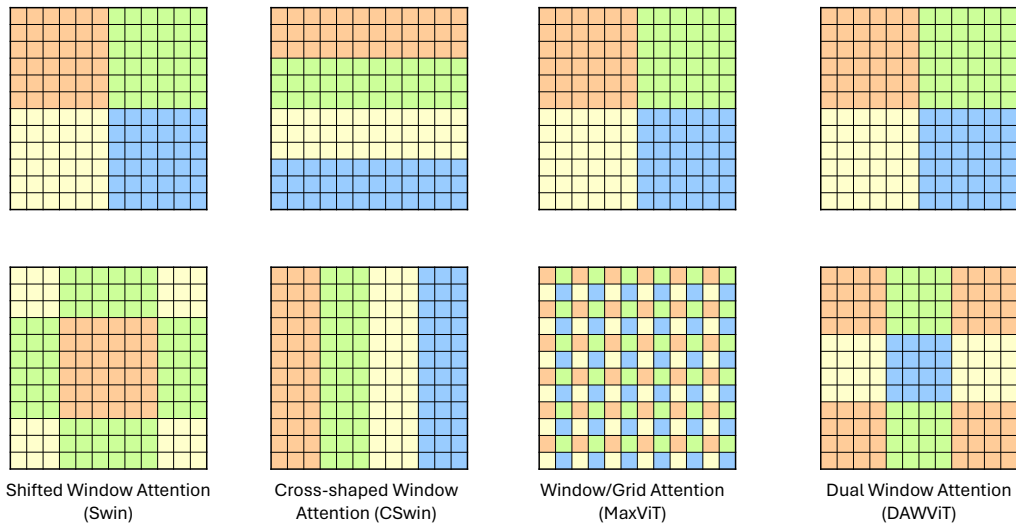

Figure 4: The comparison of our dual local window mechanism with the prior work such as the shifted local window and the cross-shaped window.

3.6 Theoretical Analysis

As aforementioned, we propose quadratic and cosine functions to model the relationships of tokens. Compared to the scale dot-product function, the difference of our method is that we map the Q and K features on the unit sphere and the relationship of tokens is only dependent on the angles between them. To better understand the angular self-attention, it is essential to investigate the relationship of tokens in our method. Thus, we provided the Proposition to analyze this problem.

Proposition 1 *Suppose the angles between the query of a token and the keys of all the tokens match $\theta_0 \leq \theta_1 \leq \cdots \leq \theta_{J-1}$. J is the total number of the tokens. In angular self-attention, the embedding of the token $\mathcal{O}_i \propto V_0 + \omega_1 V_1 + \cdots + \omega_{J-1} V_{J-1}$, where $\omega_k = \exp(\frac{s(\theta_k) - s(\theta_0)}{\tau}) \in (0, 1)$. $s(\theta) = 1 - \frac{4\theta^2}{\pi^2}$ for quadratic self-attention and $s(\theta) = \cos\theta$ for cosine self-attention.*

The proposition states that the embedding of a token can be regarded as the combination of the value vectors with the relative weight denoted by w_k. The relative weight of the value vector with the smallest angle to the target query is normalized to 1. And the relative weight of a value vector is smaller if the corresponding angle is larger. The proposition suggests the larger contribution of the value vector to the embedding of the target token with smaller angles between them. The proof can be found in Appendix.

3.7 Comparison with Prior Work

The local window mechanism has been widely adopted in various vision transformers. In different vision transformers, the local window mechanism is featured by their unique partition of the feature maps as well as the dynamic interaction of the tokens from different local windows. Fig. 4 illustrates our dual local window as well as the previous local window mechanisms. Swin Transformers (Liu et al., 2021) first proposed the shifted local window to reduce the time complexity of the vision transformer. To tackle the lack of the connection of the local windows, some techniques such as cyclic shift is adopted to adjust the partition of the local windows and the connection can be bridged in the alternating layers of the model. Another local window mechanism called Cross-Shaped Window (Dong et al., 2022) is proposed by CSwin Transformers (Dong et al.,

2022). Different from the local window partition in Swin Transformers (Liu et al., 2021), the feature map is splitted into vertical and horizontal strips in parallel and the width of the strips would determine the level of connection of tokens. Recently, Neighborhood Attention (Hassani et al., 2023) proposed the efficient and scalable sliding local window mechanism in which the attention operation is confined in a small sliding local window. Besides, MaxViT (Tu et al., 2022) proposed block attention and grid attention, respectively. The block attention performs the self-attention in the local window while the grid attention would attend to tokens globally. Furthermore, DaViT (Ding et al., 2022) also introduced channel group attention to remedy the lack of connection between the spatial local windows.

In our dual local window, the feature map is partitioned into local windows of different sizes at each layer. Compared to the prior local window mechanism such MaxViT (Tu et al., 2022) that deals with connection of local windows by grid attention, the lack of connection of local windows is mitigated by the overlapping part of the local windows in the alternating layer of the model. Besides, our dual local window enjoys three merits that are not possessed by prior work such as Swin Transformers (Liu et al., 2021) and CSwin Transformers (Dong et al., 2022) First, the partition of the local window is implemented on the queries and keys, not on the feature maps directly, which would be helpful for the direct interaction of the tokens. Second, the size of our local window is flexible. And we can choose the optimal window size for tasks with different input resolutions such as segmentation. Last but not least, our dual local window is easy to implement.

Self-attention mechanism is the core of transformers and previous work (Wang et al., 2018; Zhao et al., 2020) has shown that in the attention mechanism the similarity can be modeled by different functions and scaled dot-product function is not the only choice to model the relationship of tokens. To alleviate the large computation complexity in scaled dot product self-attention, XciT (Ali et al., 2021) proposed cross-variance attention in which the attention scores are obtained from the cross-covariance matrix computed over the key and query. Besides, Qin et. al. (Qin et al.) proposed a new variant linear transformer called Cosformer (Qin et al.). The core of Cosformer (Qin et al.) is the linearized self-attention in which the similarity score is modeled by the linear kernel function (e.g., ReLU). Furthermore, Lu et.al. (Lu et al., 2021) proposed a softmax-free transformer (SOFT) (Lu et al., 2021). In SOFT (Lu et al., 2021) the Gaussian kernel is adopted to model the interaction of the tokens and a novel low-rank matrix decomposition algorithm is proposed for approximation to reduce the computation overhead. In our angular self-attention, we suggest that the norm of the tokens play an insignificant role in the self-attention and the relationship of the tokens can be solely determined by the angles between them. As a consequence, we propose the angular self-attention in which the attention scores are obtained from our angular function and the impact from the norm of the tokens can be diminished. In order to reduce the computational cost, the linear function is adopted to approximate the time-consuming operation in the angular self-attention. The extensive experiments suggest that our angular self-attention can also successfully model the relationships of the tokens and serve as the competitor for the scaled dot product attention and linearized attention.

4 Experiments

In this section, we evaluate our proposed DWAViT on ImageNet-1K (Deng et al., 2009) classification, COCO (Lin et al., 2014) object detection, and ADE20K (Zhou et al., 2017) semantic segmentation. Besides, we also implement the ablation study to investigate the effectiveness of angular self-attention and compare the results of angular self-attention against that of traditional scaled dot-product self-attention on benchmarks.

4.1 ImageNet-1K Classification

In this experiment we adopt the same training recipe as previous work (Touvron et al., 2021a; Li et al., 2022; Lee et al., 2022; Dong et al., 2022) for fair comparison. The training strategies include repeated data augmentation methods and the EMA (Polyak & Juditsky, 1992). The total training epoch is 300 with the first 20 epochs as warm-up. We adopt the AdamW (Kingma & Ba, 2014) algorithm to optimize the model. The initial learning rate is 1.2e-3 and the weight decay is 0.05. The learning rate is adjusted according to the cosine learning rate schedule. The drop path rate is 0.1 and the input image is resized to 224×224. The mlp ratio for all the DWAViT variants is set to 4. The number of windows in each stage is (100,49), (49,16), (4,1), (1,1). The temperature in an angular self-attention is 0.1 for DWAViT-T and DWAViT-S

Table 2: The performance of our proposed DWAViT and the baseline models on the ImageNet-1K classification. The DWAViT consists of the angular self-attention and dual local windows. The resolution of the image is 224×224. The inference time is evaluated on NVIDIA A100 when the batch size is fixed at 100. [cos] and [quad] denote cosine and quadratic function, respectively.

Model	#Param(M)	#FLOPs(G)	#Inference(s)	CNN	ViT	Top-1 Acc
ResNet-50 (He et al., 2016)	25.0	4.1	205.01	✓		76.2
DeiT-S (Touvron et al., 2021a)	22.1	4.5	201.16		✓	79.8
PVT-S (Wang et al., 2021)	24.5	3.8	217.51		✓	79.8
RegNetY-4G (Radosavovic et al., 2020)	21.0	4.0	194.54	✓		80.0
CrossViT-S (Chen et al., 2021)	26.7	5.6	208.11		✓	81.0
TNT-S (Han et al., 2021)	23.8	5.2	213.60		✓	81.3
Swin-T (Liu et al., 2021)	28.3	4.5	211.91		✓	81.2
CoAtNet-0 (Dai et al., 2021)	25.0	4.0	214.64	✓		81.6
CvT-13 (Wu et al., 2021)	20.0	4.5	213.26		✓	81.6
CaiT–XS-24 (Touvron et al., 2021b)	26.6	5.4	213.11		✓	81.8
ViL-S (Zhang et al., 2021)	24.6	5.1	202.83		✓	82.0
PVTv2-B2 (Wang et al., 2022b)	25.4	4.0	218.47		✓	82.0
ConvNeXt-T (Liu et al., 2022b)	29.0	5.0	203.89	✓		82.1
HiViT-T (Zhang et al., 2022b)	19.0	4.6	213.71		✓	82.1
DaViT-T (Ding et al., 2022)	28.3	4.5	218.67		✓	**82.8**
MViTv2-T (Li et al., 2022)	24.0	4.7	217.27		✓	82.3
CSWin-T (Dong et al., 2022)	23.0	4.3	210.46		✓	<u>82.7</u>
DWAViT-T[cos] (Ours)	22.7	4.2	216.24		✓	<u>82.7</u>
DWAViT-T[quad] (Ours)	22.7	4.2	216.90		✓	**82.8**
ResNet-101 (He et al., 2016)	45.0	7.9	210.12	✓		77.4
PVT-M (Wang et al., 2021)	44.2	6.7	222.54		✓	81.2
RegNetY-8G (Radosavovic et al., 2020)	39.0	8.0	201.64	✓		81.7
Swin-S (Liu et al., 2021)	49.6	8.7	216.56		✓	83.1
CoAtNet-1 (Dai et al., 2021)	42.0	8.0	218.24	✓		83.3
CvT-21 (Wu et al., 2021)	32.0	7.1	218.60		✓	82.5
ViL-M (Zhang et al., 2021)	39.7	9.1	208.04		✓	83.3
PVTv2-B3 (Wang et al., 2022b)	45.2	6.9	226.60		✓	83.2
ConvNeXt-S (Liu et al., 2022b)	50.0	9.0	207.71	✓		83.1
Focal-S (Yang et al., 2021)	51.1	9.1	230.70		✓	<u>83.5</u>
HiViT-S (Zhang et al., 2022b)	38.0	9.1	221.46		✓	<u>83.5</u>
MViTv2-S (Li et al., 2022)	35.0	7.0	224.71		✓	**83.6**
CSWin-S (Dong et al., 2022)	35.0	6.9	213.72		✓	**83.6**
DWAViT-S[cos] (Ours)	44.6	8.2	218.81		✓	<u>83.5</u>
DWAViT-S[quad] (Ours)	44.6	8.2	219.38		✓	**83.6**
ResNet-152 (He et al., 2016)	60.0	11.0	216.37	✓		78.3
PVT-L (Wang et al., 2021)	61.4	9.8	227.47		✓	81.7
DeiT-B (Touvron et al., 2021a)	86.7	17.4	206.01		✓	81.8
Swin-B (Liu et al., 2021)	87.8	15.4	219.12		✓	83.4
ViL-B (Zhang et al., 2021)	55.7	13.4	210.63		✓	83.2
Focal-B (Yang et al., 2021)	89.8	16.0	235.18		✓	<u>83.8</u>
HiViT-B (Zhang et al., 2022b)	66.0	15.9	225.62		✓	<u>83.8</u>
DWAViT-B[cos] (Ours)	77.4	14.3	220.36		✓	**83.9**
DWAViT-B[quad] (Ours)	77.4	14.3	223.21		✓	<u>83.8</u>

Table 3: Object detection and instance segmentation performance of our model and the baseline models with Mask R-CNN framework. The DWAViT consists of the angular self-attention and dual local windows. The model is trained with a 3x scheme. The FLOPs are measured at resolution 800×1280. The inference time is evaluated on NVIDIA A100 when the batch size is fixed at 100. [cos] and [quad] denote cosine and quadratic function, respectively.

Backbone	#Param(M)	#FLOPs(G)	#Inference(s)	AP^b	AP^b_{50}	AP^b_{75}	AP^m	AP^m_{50}	AP^m_{75}
ResNet-50 (He et al., 2016)	44	260	138.23	41.0	61.7	44.9	37.1	58.4	40.1
ConvNeXt-T (Liu et al., 2022b)	48	262	163.04	46.2	67.9	50.8	41.7	65.0	44.9
PVT-S (Wang et al., 2021)	44	245	177.20	43.0	65.3	46.9	39.9	62.5	42.8
ViL-S (Zhang et al., 2021)	45	218	-	47.1	68.7	51.5	42.7	65.9	46.2
TwinsP-S (Chu et al., 2021a)	44	245	-	46.8	69.3	51.8	42.6	66.3	46.0
Twins-S (Chu et al., 2021a)	44	228	-	46.8	69.2	51.2	42.6	66.3	45.8
Swin-T (Liu et al., 2021)	48	264	194.50	46.0	68.2	50.2	41.6	65.1	44.8
Focal-T (Yang et al., 2021)	49	291	-	47.2	69.4	51.9	42.7	66.5	45.9
PVTv2-B2 (Wang et al., 2022b)	45	309	210.43	47.8	69.7	52.6	43.1	66.8	46.7
XciT-S12/8 (Ali et al., 2021)	43	550	233.54	47.0	68.9	51.7	42.3	66.0	45.4
DaViT-T (Ding et al., 2022)	48	263	244.08	47.4	69.5	52.0	42.9	66.8	46.4
DAT-T (Xia et al., 2022)	48	272	-	47.1	69.2	51.6	42.4	66.1	45.5
MViTv2-T (Li et al., 2022)	44	279	206.42	48.2	**70.9**	53.3	**43.8**	<u>67.9</u>	**47.2**
NAT-T (Hassani et al., 2023)	48	258	157.28	47.7	69.0	52.6	42.6	66.1	45.9
GC ViT-T (Hatamizadeh et al., 2023)	48	291	240.19	47.9	70.1	52.8	43.2	67.0	46.7
DWAViT-T[cos] (Ours)	42	255	223.46	<u>48.4</u>	70.4	<u>53.1</u>	<u>43.5</u>	67.7	<u>47.1</u>
DWAViT-T[quad] (Ours)	42	255	235.47	**48.8**	<u>70.7</u>	**53.6**	**43.8**	68.1	<u>47.1</u>
Res101 (He et al., 2016)	63	336	155.50	42.8	63.2	47.1	38.5	60.1	41.3
ConvNeXt-S (Liu et al., 2022b)	70	348	225.28	47.9	70.0	52.7	42.9	66.9	46.2
PVT-M (Wang et al., 2021)	64	302	222.18	44.2	66.0	48.2	40.5	63.1	43.5
ViL-M (Zhang et al., 2021)	60	261	-	44.6	66.3	48.5	40.7	63.8	43.7
TwinsP-B (Chu et al., 2021a)	64	302	-	47.9	70.1	52.5	43.2	67.2	46.3
Twins-B (Chu et al., 2021a)	76	340	-	48.0	69.5	52.7	43.0	66.8	46.6
Swin-S (Liu et al., 2021)	69	354	222.31	48.5	70.2	53.5	43.3	67.3	46.6
Focal-S (Yang et al., 2021)	71	401	-	<u>48.8</u>	<u>70.5</u>	<u>53.6</u>	<u>43.8</u>	<u>67.7</u>	<u>47.2</u>
PVTv2-B3 (Wang et al., 2022b)	65	397	265.97	48.4	69.8	53.3	43.2	66.9	46.7
XCiT-M24/8 (Ali et al., 2021)	99	1448	467.60	48.5	70.3	53.4	43.7	67.5	46.9
NAT-S (Hassani et al., 2023)	70	330	204.44	48.4	69.8	53.2	43.2	66.9	46.5
DWAViT-S[cos] (Ours)	64	338	268.51	48.4	70.0	53.3	43.6	67.4	47.0
DWAViT-S[quad] (Ours)	64	338	282.52	**49.1**	**70.8**	53.5	**44.0**	**68.2**	**47.4**
X101-64 (Xie et al., 2017)	101	493	207.68	44.4	64.9	48.8	39.7	61.9	42.6
PVT-L (Wang et al., 2021)	81	364	286.52	44.5	66.0	48.3	40.7	63.4	43.7
Swin-B (Liu et al., 2021)	107	496	393.74	48.5	69.8	53.2	43.4	66.8	<u>46.9</u>
DaViT-B (Ding et al., 2022)	107	491	461.84	**49.9**	**71.5**	<u>54.6</u>	**44.6**	**68.8**	47.8
DWAViT-B[cos] (Ours)	97	462	423.62	<u>49.8</u>	<u>71.2</u>	54.8	<u>44.5</u>	<u>68.6</u>	47.8
DWAViT-B[quad] (Ours)	97	462	440.69	49.4	71.1	<u>54.6</u>	44.4	<u>68.6</u>	**47.8**

and 0.25 for DWAViT-B, respectively. The linear function is adopted to simplify the computation of the quadratic self-attention and τ is set to 0.4. All the experiments are running on NVIDIA A100. To evaluate the time efficiency of our proposed model, the inference time is also reported. Since the model is trained on ImageNet-1K for many training epochs (300 epochs), the variance could be diminished considerably and become insignificant compared to the main results. Thus, only the major results are reported.

The results are illustrated in Table 2. Our proposed DWAViT is compared against the previous state-of-the-art vision transformers and CNNs including the CSwin (Dong et al., 2022), MViTv2 (Li et al., 2022), DaViT (Ding et al., 2022) and ConvNeXt (Liu et al., 2022b). Specifically, Swin Transformer (Liu et al., 2021), Focal Transformer (Yang et al., 2021), DaViT (Ding et al., 2022), MViTv2 (Li et al., 2022) and CSWin Transformer (Dong et al., 2022) are baselines for the exact comparison. The experimental results show that under the similar amount of parameters, the DWAViT-T can outperform the latest vision transformers and CNNs, The top-1 accuracy of the DWAViT-T can achieve 82.8%, which is even 0.1% higher than that of CSwin-T (Dong et al., 2022). As for the small-sized model, our DWAViT-S can achieve the top-1 accuracy of 83.6% in the classification task, which is on par with that of CSWin (Dong et al., 2022) and MViTv2 (Li et al., 2022). For base-sized models, our DWAViT-B with cosine self-attention can achieve 83.9% accuracy in the ImageNet-1K classification task.

Table 4: The semantic segmentation performance of DWAViT-T and baselines on ADE20K. The FLOPs are calculated with resolution 512×2048. [cos] and [quad] denote cosine and quadratic function, respectively.

Backbone	#Param(M)	#FLOPs(G)	mIoU
Swin-T (Liu et al., 2021)	59	945	44.5
Focal-T (Yang et al., 2021)	62	998	45.8
XciT-S12/16 (Ali et al., 2021)	54	966	45.9
XciT-S12/8 (Ali et al., 2021)	53	1237	46.6
DaViT-T (Ding et al., 2022)	60	940	46.3
DAT-T (Xia et al., 2022)	60	957	45.5
GC ViT-T (Hatamizadeh et al., 2023)	58	947	47.0
NAT-T (Hassani et al., 2023)	58	934	<u>47.1</u>
DWAViT-T[cos] (Ours)	52	930	**47.5**
DWAViT-T[quad] (Ours)	52	930	45.4

4.2 COCO Object Detection

Next, we evaluate our model on the COCO object detection task. The COCO dataset has 118K images for training and 5K images for validation. We adopt the Mask R-CNN (He et al., 2017) and Cascade Mask R-CNN (Cai & Vasconcelos, 2018) as the framework and our DWAViT serves as the backbone. For a fair comparison, we follow the same training recipe as the previous work (Touvron et al., 2021a; Li et al., 2022; Lee et al., 2022; Dong et al., 2022) and perform the experiment with MMDetection toolbox (Chen et al., 2019). In order to tackle the images with high resolution. The number of local windows in the object detection task is different from that in the image classification task. The number of windows in each stage is (256,225), (64,49), (16,9), (4,1), respectively. In both frameworks, the size of the local window in each stage is half of that in the previous stage. We use the model pretrained on ImageNet-1K and fine-tune it on the COCO dataset with $1\times$ and $3 \times$ schedule with 12 and 36 epochs, respectively.

The results on object detection and instance segmentation of our our model and the baseline models with Mask R-CNN (He et al., 2017) framework with $3\times$ schedule are illustrated in Table 3. The baseline methods include the latest ViT models such as MViTv2 (Li et al., 2022), DAT (Xia et al., 2022) and DAViT (Xia et al., 2022).Specifically, Swin Transformer (Liu et al., 2021), Focal Transformer (Yang et al., 2021), XciT (Ali et al., 2021), DAT (Xia et al., 2022) and CSwin (Dong et al., 2022) are baselines for exact comparison. The experimental results show that the DWAViT can achieve on par or better result with latest baseline methods. For DWAViT-T, the AP^b can achieve 48.8%, which is 0.4% higher than that of MViTv2-T (Li et al., 2022). the AP_m of DWAViT-T is 43.8%, which is on par with that of MViTv2-T (Li et al., 2022). The DWAViT-S achieves 49.1% on AP^b and 44.4% on AP^m, which outperforms all the baseline methods. And the experimental results suggest that our DWAViT-B can outperform the Swin-B (Liu et al., 2021) on this task. More results can be found in Appendix.

4.3 ADE20K Semantic Segmentation

In this section, we further investigate the performance of our proposed model on semantic segmentation task. The Upernet (Xiao et al., 2018) framework is adopted. Our model and the baseline methods are evaluated on benchmark ADE20K (Zhou et al., 2017). For fair comparison, we follow the training procedure from previous works (Ding et al., 2022; Dong et al., 2022) and perform the experiment with MMSegmentation toolbox (Contributors, 2020). The image is resized to 512×512 and train the model with 160K iterations. the mIoU is adopted as the metric. The results of experiment are illustrated in Table 4 and Table 15 (see Appendix). Swin Transformer (Liu et al., 2021), Focal Transformer (Yang et al., 2021), XciT (Ali et al., 2021), DaViT (Xia et al., 2022) and DAT (Xia et al., 2022) are the baselines for exact comparison. Those methods are also implemented with MMSegmentation toolbox (Contributors, 2020). Besides, Upernet (Xiao et al., 2018) is adopted as the framework and models pre-trained on ImageNet-1K only are used as the feature extractor for the baselines and our method. The results show that our DWAViT with cosine self-attention function can outperform the baselines. Besides, the performance of our model with cosine function is also much better than that of our model with quadratic function. The mIoU of DWAViT-T can reach 47.5% ,

Table 5: The performance of our proposed DWAViT with angular self-attention, scaled dot-product self-attention and the linearized self-attention on the ImageNet-1K classification. The resolution of the image is 224 × 224.

Model	Param(M)	FLOPs(G)	Top-1 Acc
DWAViT-T[dot product]	22.7	4.2	82.5
DWAViT-T[linear]	22.7	4.2	82.2
DWAViT-T[cos] (Ours)	22.7	4.2	82.7
DWAViT-T[quad] (Ours)	22.7	4.2	**82.8**

Table 6: The performance of our proposed DWAViT with the dual local window, window/grid attention and the shifted local window on the ImageNet-1K classification. We adopt the quadratic self-attention and the resolution of the image is 224 × 224.

Backbone	Param(M)	FLOPs(G)	Top-1 Acc
DWAViT-T[shifted window]	22.7	4.2	82.4
DWAViT-T[window/grid]	22.7	4.2	82.5
DWAViT-T[dual window] (Ours)	22.7	4.2	**82.8**

Table 7: Object detection and instance segmentation performance of our DWAViT with angular self-attention, scaled dot-product self-attention and linearized self-attention in Mask R-CNN framework. The model is trained with a 3x scheme. The FLOPs are measured at resolution 800 × 1280.

Backbone	#Param(M)	#FLOPs(G)	AP^b	AP^b_{50}	AP^b_{75}	AP^m	AP^m_{50}	AP^m_{75}
DWAViT-T[dot product]	42	255	48.4	70.3	53.2	43.5	67.5	**47.1**
DWAViT-T[linear]	42	255	48.0	70.0	52.8	43.2	67.0	46.5
DWAViT-T[cos] (Ours)	42	255	48.4	70.4	53.1	43.5	67.7	**47.1**
DWAViT-T[quad] (Ours)	42	255	**48.8**	**70.7**	**53.6**	**43.8**	**68.1**	**47.1**

Table 8: Object detection and instance segmentation performance of our DWAViT with the dual local window, shifted local window and window/grid attention in Mask R-CNN framework. The model is trained with a 3x scheme. We adopt the quadratic self-attention and the FLOPs are measured at resolution 800 × 1280.

Backbone	#Param(M)	#FLOPs(G)	AP^b	AP^b_{50}	AP^b_{75}	AP^m	AP^m_{50}	AP^m_{75}
DWAViT-T[shifted window]	42	259	47.5	69.1	52.3	42.5	66.3	45.9
DWAViT-T[window/grid]	42	259	47.8	70.2	52.7	42.9	66.7	46.3
DWAViT-T[dual window] (Ours)	42	255	**48.8**	**70.7**	**53.6**	**43.8**	**68.1**	**47.1**

Table 9: The performance of Swin-T, DeiT-S, CSwin-T and MaxViT-T with angular self-attention and scaled dot-product self-attention on the ImageNet-1K classification. The resolution of the image is 224 × 224. The dot product, cos and quad in the square bracket denote scaled dot-product, cosine and quadratic function, respectively.

Model	Param(M)	FLOPs(G)	Top-1 Acc
Swin-T (Liu et al., 2021) [dot product]	28	4.3	81.2
Swin-T (Liu et al., 2021) [cos] (Ours)	28	4.3	**81.4**
Swin-T (Liu et al., 2021) [quad] (Ours)	28	4.3	81.3
DeiT-S (Touvron et al., 2021a) [dot product]	22	4.6	79.8
DeiT-S (Touvron et al., 2021a) [cos] (Ours)	22	4.6	80.0
DeiT-S (Touvron et al., 2021a) [quad] (Ours)	22	4.6	**80.2**
CSwin-T (Dong et al., 2022)[dot product]	23	4.3	82.7
CSwin-T (Dong et al., 2022)[cos] (Ours)	23	4.3	82.9
CSwin-T (Dong et al., 2022)[quad] (Ours)	23	4.3	**83.0**
MaxViT-T (Tu et al., 2022)[dot product]	31	5.6	83.6
MaxViT-T (Tu et al., 2022)[cos] (Ours)	31	5.6	**83.8**
MaxViT-T (Tu et al., 2022)[quad] (Ours)	31	5.6	**83.8**

which outperforms other baseline methods like DAT-T (Xia et al., 2022), DaViT-T (Ding et al., 2022) and XciT-S (Ali et al., 2021).
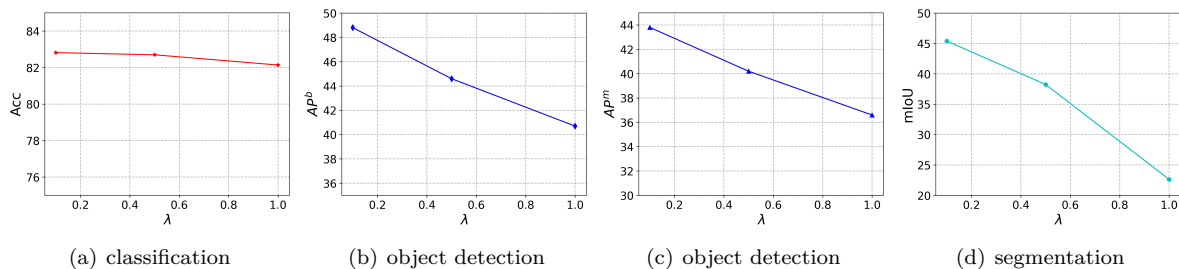
(a) classification | (b) object detection | (c) object detection | (d) segmentation

Figure 5: The performance of our model with different values of λ on classification, object detection and segmentation tasks.

Table 10: The actual running time of Swin Transformer and our DWAViT during the training on ImageNet-1K. We implement the testing on a single A100 GPU and the batch size is fixed to 100 for all the models. The average time per iteration is reported.

Model	#Param(M)	#FLOPs(G)	Inference($\times 10^{-2}$ s)	Training(s)
Swin-T (Liu et al., 2021)	28.3	4.5	4.6	0.15
DWAViT-T[cos](Ours)	22.7	4.2	3.6	0.20
DWAViT-T[quad] (Ours)	22.7	4.2	4.0	0.20
Swin-S (Liu et al., 2021)	49.6	8.7	7.1	0.23
DWAViT-S[cos](Ours)	44.6	8.2	6.9	0.29
DWAViT-S[quad] (Ours)	44.6	8.2	7.4	0.31
Swin-B (Liu et al., 2021)	87.8	15.4	9.2	0.30
DWAViT-B[cos](Ours)	77.4	14.3	9.6	0.40
DWAViT-B[quad] (Ours)	77.4	14.3	10.3	0.42

4.4 Running Time Analysis

In this section we quantitatively evaluate the actual running time of our model in both training and inference stages on the image classification task. Specifically, we fix the batch to 100 and compare the running time of our model with that of Swin Transformer (Liu et al., 2021). All the experiments are implemented on a single A100 GPU and we report the average time per iteration and the results are illustrated in Table 10. The experimental results suggest that our model could achieve comparable inference time with that of Swin Transformer (Liu et al., 2021). Specifically, compared to Swin-T (Liu et al., 2021), our DWAViT-T(cos) can achieve 1.5% higher accuracy on image classification with lower time cost during the inference stage. Our DWAViT-B(cos) can achieve an improvement of 0.5% in accuracy on the classification task with almost the same inference time of Swin-B Liu et al. (2021). Basically, the time cost of our model with quadratic self-attention would be slightly higher than that of our model with cosine self-attention. Besides, the training time of our model is slightly higher than that of Swin Transformer (Liu et al., 2021) due to the new formulation in self-attention. However, the actual running time does not blow up when the size of our model scales up.

4.5 Ablation Study

In the ablation study we first compare the performance of our model with traditional scaled dot-product self-attention and our proposed angular self-attention. In the experiment we replace the angular self-attention with traditional scaled dot-product self-attention or linearized self-attention and evaluate the performance of the model on ImageNet-1K classification, COCO object detection and ADE20K semantic segmentation. We adopt the DWAViT-T as the backbone in three tasks. The results of the image classification and objection detection are illustrated in Table 5 and Table 7, respectively. More results on other tasks can be found in Appendix. When our model adopts the traditional scaled dot-product self-attention, the top-1 accuracy would be 0.2% and 0.3% lower than that of cosine function and quadratic function. On the object detection task our angular self-attention also achieves better performance than that of the baseline methods. We further investigate the performance of our angular self-attention by replacing the scaled dot-product self-attention

with our angular self-attention in other vision transformer models. Table 9 shows the performance of Swin-T (Liu et al., 2021), DeiT-S (Touvron et al., 2021a), CSWin-T (Dong et al., 2022) and MaxViT-T (Tu et al., 2022) ImageNet-1K image classification with scaled dot-product self-attention and our proposed angular self-attention. The experimental results suggest that when the existing vision transformer models are equipped with our angular self-attention, the performance on the image classification can be improved. It further validates that our angular self-attention is a competitive alternative for the scaled dot-product self-attention.

We also compare the performance of our model with the proposed dual local window with the shifted window proposed by Swin Transformer (Liu et al., 2021) and the window/grid attention from MaxViT (Tu et al., 2022). In the experiment we replace the dual local window with the shifted local window and window/grid attention and evaluate the performance of the model on ImageNet-1K classification, COCO object detection and ADE20K semantic segmentation. We adopt the DWAViT-T(quad) as the backbone in three tasks. The results of the image classification and object detection are illustrated in Table 6 and Table 8. More results on other tasks can be found in Appendix. When our model is equipped with the shifted local window, the top-1 accuracy would be 0.4% lower than that of the model with our proposed dual local window. On the object detection task, our dual local window also achieves better performance than that of baseline methods, which suggests our dual local window is a strong competitor to the shifted local window and window/grid attention.

At last, We investigate the effect of the hyper-parameter on the performance of our model. The temperature scaling coefficient λ is the primary hyper-parameter in our angular self-attention and it determines the discriminativeness of the similarity score of tokens. We adopt DWAViT-T̃(quad) as the target model and choose 0.1, 0.5,1.0 as the value of λ. The performance of the model is evaluated on image classification, object detection and semantic segmentation and the results are shown in Fig 5. The results suggest that the performance of our model would be reduced with larger value of λ. Compared to the classification task, the performance of our model is more sensitive to the change of the value of λ. Since the value of λ become larger, the similarity score of the tokens would become less discriminative. And the ability of our angular self-attention to model the interaction of tokens would be undermined. As a consequence, the performance of the model would drop, especially on object detection and segmentation tasks.

4.6 Statistical Significance

To validate the statistical significance of our results on various tasks (classification, object detection and segmentation), we perform the significant test on our proposed DWAViT model and choose one important baseline model (e.g., Swin Transformer (Liu et al., 2021)) for the comparison. In image classification the Swin-T (Liu et al., 2021) is adopted in our test. The average accuracy of Swin-T (Liu et al., 2021) is 81.20% as reported in the original paper. To demonstrate that the performance improvement of our proposed model is statistically significant over that of Swin Transformer. We first choose DWAViT-T

Table 11: The results of the significant test on classification, objection detection and segmentation tasks.

Task	t-score	p-value
Classification	1477.27	7.65e-50
Object detection	245.76	4.81e-35
Segmentation	369.16	2.11e-38

as the target model since it has similar size with that of Swin-T. Our null hypothesis is acc(DWAViT-T) acc(Swin-T) and the alternative hypothesis is acc(DWAViT-T) > acc(Swin-T). Next, the evaluation of our model on image classification is performed multiple times (e.g., 20) under different settings. At last, the t-score and p-value are calculated according to the one-tail T-test and the result is shown in Table 11. The p-value is 7.65e-50, which is significantly smaller than the threshold 0.05. For object detection and segmentation tasks, we follow the same routine and the results are also shown in Table 11. The results suggest the rejection of the null hypothesis and the improvements of our proposed model are statistically significant.

Our experimental results show that when the scaled dot-product self-attention in CSwin (Dong et al., 2022) and MaxViT (Tu et al., 2022) is placed by our angular self-attention. There is a slight performance improvement in the image classification, as illustrated in Table 9. To further validate the statistical significance of the improvement, we perform the significant test

Table 12: The results of the significant test on CSwin and MaxViT.

Model	t-score	p-value
CSwin-T (Dong et al., 2022)	144.47	1.16e-30
MaxViT-T (Tu et al., 2022)	96.55	2.42e-27

on CSwin (Dong et al., 2022) and MaxViT (Tu et al., 2022) with our angular self-attention, respectively. In the test, the CSwin-T (Dong et al., 2022) is chosen as the target model and the null hypothesis would be that the performance of CSwin (Dong et al., 2022) with our angular self-attention (quad) is less than that of CSwin (Dong et al., 2022) with scaled dot-product self-attention, namely $\text{acc}(\text{CSwin}(\text{quad})) \leq \text{acc}(\text{CSwin}(\text{dot-product})) = 82.7\%$. Next, the evaluation of CSwin with our angular self-attention on image classification is performed multiple times (e.g., 20) under different settings (e.g., different seeds). At last, the t-score and p-value are also calculated according to the one-tail T-test and the results of CSwin (Dong et al., 2022) are shown in Table 12. The p-value for CSwin (Dong et al., 2022) is 1.16e-39, which is significantly smaller than the threshold 0.05. The results suggest that the null hypothesis should be rejected. We follow the same routine to perform the hypothesis test on MaxViT (Tu et al., 2022) and the results are also illustrated in Table 12. Both results suggest that the improvement on the image classification is indeed statistically significant and our angular self-attention can serve as a strong competitor for the traditional scaled dot-product self-attention.

5   Conclusions

In this paper, we propose the dual-window mechanism and angular self-attention. The dual-window mechanism divides the feature maps into even/odd numbers of local windows in each stage alternatively for the information exchange of the local windows. In angular self-attention, the traditional scaled dot-product operation is replaced by our proposed quadratic and cosine functions. The proposed angular function can also model the relationship of tokens in the long range. Based on the dual-window mechanism and angular self-attention, we propose a new vision transformer backbone called dual-windowed angular vision transformer. Extensive experiments show that our backbone can achieve competitive performance on the tasks such as image classification, object detection and semantic segmentation and while maintaining the comparable computational cost with that of the baseline models.

Broader Impact. This work proposed a new architecture of vision transformer called DWAViT featured by angular self-attention and dual local window mechanism. Our model is proven to achieve competitive performance in downstream tasks such as object detection and semantic segmentation and has the enormous potential to be used in various practical scenarios. In particular, object detection is one of the most promising applications of vision transformers in the real world and it is often used in systems which require extensive interaction with the surrounding environment visually. For instance, autonomous vehicles require a large number of object detectors to identify the pedestrians and other vehicles nearby and the safety and the trustworthiness of vision transformers are critical in this area. Though our proposed model can achieve promising results on object detection and other tasks, some critical issues such as adversarial robustness and trustworthiness are quite under-explored and further investigation is necessarily required.

Acknowledgement

References

Alaaeldin Ali, Hugo Touvron, Mathilde Caron, Piotr Bojanowski, Matthijs Douze, Armand Joulin, Ivan Laptev, Natalia Neverova, Gabriel Synnaeve, Jakob Verbeek, et al. Xcit: Cross-covariance image transformers. *Advances in neural information processing systems*, 34:20014–20027, 2021.

Zhaowei Cai and Nuno Vasconcelos. Cascade r-cnn: Delving into high quality object detection. In *Proceedings of the IEEE Conference on Computer Vision and Pattern Recognition (CVPR)*, June 2018.

Nicolas Carion, Francisco Massa, Gabriel Synnaeve, Nicolas Usunier, Alexander Kirillov, and Sergey Zagoruyko. End-to-end object detection with transformers. In *Computer Vision–ECCV 2020: 16th European Conference, Glasgow, UK, August 23–28, 2020, Proceedings, Part I 16*, pp. 213–229. Springer, 2020.

Chun-Fu Richard Chen, Quanfu Fan, and Rameswar Panda. Crossvit: Cross-attention multi-scale vision transformer for image classification. In *Proceedings of the IEEE/CVF international conference on computer vision*, pp. 357–366, 2021.

Kai Chen, Jiaqi Wang, Jiangmiao Pang, Yuhang Cao, Yu Xiong, Xiaoxiao Li, Shuyang Sun, Wansen Feng, Ziwei Liu, Jiarui Xu, et al. Mmdetection: Open mmlab detection toolbox and benchmark. *arXiv preprint arXiv:1906.07155*, 2019.

Liyan Chen, Weihan Wang, and Philippos Mordohai. Learning the distribution of errors in stereo matching for joint disparity and uncertainty estimation. In *Proceedings of the IEEE/CVF Conference on Computer Vision and Pattern Recognition (CVPR)*, pp. 17235–17244, June 2023a.

Mengzhao Chen, Mingbao Lin, Ke Li, Yunhang Shen, Yongjian Wu, Fei Chao, and Rongrong Ji. Cf-vit: A general coarse-to-fine method for vision transformer. In *Proceedings of the AAAI Conference on Artificial Intelligence*, volume 37, pp. 7042–7052, 2023b.

Yinpeng Chen, Xiyang Dai, Dongdong Chen, Mengchen Liu, Xiaoyi Dong, Lu Yuan, and Zicheng Liu. Mobile-former: Bridging mobilenet and transformer. In *Proceedings of the IEEE/CVF Conference on Computer Vision and Pattern Recognition*, pp. 5270–5279, 2022.

François Chollet. Xception: Deep learning with depthwise separable convolutions. In *Proceedings of the IEEE conference on computer vision and pattern recognition*, pp. 1251–1258, 2017.

Krzysztof Marcin Choromanski, Valerii Likhosherstov, David Dohan, Xingyou Song, Andreea Gane, Tamas Sarlos, Peter Hawkins, Jared Quincy Davis, Afroz Mohiuddin, Lukasz Kaiser, et al. Rethinking attention with performers. In *International Conference on Learning Representations*.

Xiangxiang Chu, Zhi Tian, Yuqing Wang, Bo Zhang, Haibing Ren, Xiaolin Wei, Huaxia Xia, and Chunhua Shen. Twins: Revisiting the design of spatial attention in vision transformers. In *NeurIPS*, pp. 9355–9366, 2021a.

Xiangxiang Chu, Zhi Tian, Bo Zhang, Xinlong Wang, Xiaolin Wei, Huaxia Xia, and Chunhua Shen. Conditional positional encodings for vision transformers. *arXiv preprint arXiv:2102.10882*, 2021b.

MMSegmentation Contributors. Mmsegmentation: Openmmlab semantic segmentation toolbox and benchmark, 2020.

Jean-Baptiste Cordonnier, Andreas Loukas, and Martin Jaggi. On the relationship between self-attention and convolutional layers. In *International Conference on Learning Representations*, 2019.

Zihang Dai, Hanxiao Liu, Quoc V Le, and Mingxing Tan. Coatnet: Marrying convolution and attention for all data sizes. *Advances in Neural Information Processing Systems*, 34:3965–3977, 2021.

Tri Dao, Dan Fu, Stefano Ermon, Atri Rudra, and Christopher Ré. Flashattention: Fast and memory-efficient exact attention with io-awareness. *Advances in Neural Information Processing Systems*, 35:16344–16359, 2022.

Jia Deng, Wei Dong, Richard Socher, Li-Jia Li, Kai Li, and Li Fei-Fei. Imagenet: A large-scale hierarchical image database. In *2009 IEEE conference on computer vision and pattern recognition*, pp. 248–255. Ieee, 2009.

Mingyu Ding, Bin Xiao, Noel Codella, Ping Luo, Jingdong Wang, and Lu Yuan. Davit: Dual attention vision transformers. In *Computer Vision–ECCV 2022: 17th European Conference, Tel Aviv, Israel, October 23–27, 2022, Proceedings, Part XXIV*, pp. 74–92. Springer, 2022.

Xiaoyi Dong, Jianmin Bao, Dongdong Chen, Weiming Zhang, Nenghai Yu, Lu Yuan, Dong Chen, and Baining Guo. Cswin transformer: A general vision transformer backbone with cross-shaped windows. In *Proceedings of the IEEE/CVF Conference on Computer Vision and Pattern Recognition*, pp. 12124–12134, 2022.

Alexey Dosovitskiy, Lucas Beyer, Alexander Kolesnikov, Dirk Weissenborn, Xiaohua Zhai, Thomas Unterthiner, Mostafa Dehghani, Matthias Minderer, Georg Heigold, Sylvain Gelly, Jakob Uszkoreit, and Neil Houlsby. An image is worth 16x16 words: Transformers for image recognition at scale. In *ICLR*. OpenReview.net, 2021.

Haoqi Fan, Bo Xiong, Karttikeya Mangalam, Yanghao Li, Zhicheng Yan, Jitendra Malik, and Christoph Feichtenhofer. Multiscale vision transformers. In *Proceedings of the IEEE/CVF International Conference on Computer Vision*, pp. 6824–6835, 2021.

Jianyuan Guo, Kai Han, Han Wu, Yehui Tang, Xinghao Chen, Yunhe Wang, and Chang Xu. Cmt: Convolutional neural networks meet vision transformers. In *Proceedings of the IEEE/CVF Conference on Computer Vision and Pattern Recognition*, pp. 12175–12185, 2022.

Dongchen Han, Xuran Pan, Yizeng Han, Shiji Song, and Gao Huang. Flatten transformer: Vision transformer using focused linear attention. In *Proceedings of the IEEE/CVF International Conference on Computer Vision*, pp. 5961–5971, 2023.

Kai Han, An Xiao, Enhua Wu, Jianyuan Guo, Chunjing Xu, and Yunhe Wang. Transformer in transformer. *Advances in Neural Information Processing Systems*, 34:15908–15919, 2021.

Ali Hassani, Steven Walton, Jiachen Li, Shen Li, and Humphrey Shi. Neighborhood attention transformer. *arXiv preprint arXiv:2204.07143*, 2022.

Ali Hassani, Steven Walton, Jiachen Li, Shen Li, and Humphrey Shi. Neighborhood attention transformer. In *Proceedings of the IEEE/CVF Conference on Computer Vision and Pattern Recognition*, pp. 6185–6194, 2023.

Ali Hatamizadeh, Hongxu Yin, Greg Heinrich, Jan Kautz, and Pavlo Molchanov. Global context vision transformers. In *International Conference on Machine Learning*, pp. 12633–12646. PMLR, 2023.

Kaiming He, Xiangyu Zhang, Shaoqing Ren, and Jian Sun. Deep residual learning for image recognition. In *Proceedings of the IEEE conference on computer vision and pattern recognition*, pp. 770–778, 2016.

Kaiming He, Georgia Gkioxari, Piotr Dollar, and Ross Girshick. Mask r-cnn. In *Proceedings of the IEEE International Conference on Computer Vision (ICCV)*, Oct 2017.

Liqiang He and Sinisa Todorovic. Destr: Object detection with split transformer. In *Proceedings of the IEEE/CVF conference on computer vision and pattern recognition*, pp. 9377–9386, 2022.

Andrew G Howard, Menglong Zhu, Bo Chen, Dmitry Kalenichenko, Weijun Wang, Tobias Weyand, Marco Andreetto, and Hartwig Adam. Mobilenets: Efficient convolutional neural networks for mobile vision applications. *arXiv preprint arXiv:1704.04861*, 2017.

Gao Huang, Zhuang Liu, Laurens Van Der Maaten, and Kilian Q Weinberger. Densely connected convolutional networks. In *Proceedings of the IEEE conference on computer vision and pattern recognition*, pp. 4700–4708, 2017.

Zilong Huang, Xinggang Wang, Lichao Huang, Chang Huang, Yunchao Wei, and Wenyu Liu. Ccnet: Criss-cross attention for semantic segmentation. In *Proceedings of the IEEE/CVF international conference on computer vision*, pp. 603–612, 2019.

Angelos Katharopoulos, Apoorv Vyas, Nikolaos Pappas, and François Fleuret. Transformers are rnns: Fast autoregressive transformers with linear attention. In *International Conference on Machine Learning*, pp. 5156–5165. PMLR, 2020.

Diederik P Kingma and Jimmy Ba. Adam: A method for stochastic optimization. *arXiv preprint arXiv:1412.6980*, 2014.

Youngwan Lee, Jonghee Kim, Jeffrey Willette, and Sung Ju Hwang. Mpvit: Multi-path vision transformer for dense prediction. In *Proceedings of the IEEE/CVF Conference on Computer Vision and Pattern Recognition*, pp. 7287–7296, 2022.

Yanghao Li, Chao-Yuan Wu, Haoqi Fan, Karttikeya Mangalam, Bo Xiong, Jitendra Malik, and Christoph Feichtenhofer. Mvitv2: Improved multiscale vision transformers for classification and detection. In *Proceedings of the IEEE/CVF Conference on Computer Vision and Pattern Recognition*, pp. 4804–4814, 2022.

Tsung-Yi Lin, Michael Maire, Serge Belongie, James Hays, Pietro Perona, Deva Ramanan, Piotr Dollár, and C Lawrence Zitnick. Microsoft coco: Common objects in context. In *Computer Vision–ECCV 2014: 13th European Conference, Zurich, Switzerland, September 6-12, 2014, Proceedings, Part V 13*, pp. 740–755. Springer, 2014.

Ze Liu, Yutong Lin, Yue Cao, Han Hu, Yixuan Wei, Zheng Zhang, Stephen Lin, and Baining Guo. Swin transformer: Hierarchical vision transformer using shifted windows. In *Proceedings of the IEEE/CVF international conference on computer vision*, pp. 10012–10022, 2021.

Ze Liu, Han Hu, Yutong Lin, Zhuliang Yao, Zhenda Xie, Yixuan Wei, Jia Ning, Yue Cao, Zheng Zhang, Li Dong, et al. Swin transformer v2: Scaling up capacity and resolution. In *Proceedings of the IEEE/CVF conference on computer vision and pattern recognition*, pp. 12009–12019, 2022a.

Zhuang Liu, Hanzi Mao, Chao-Yuan Wu, Christoph Feichtenhofer, Trevor Darrell, and Saining Xie. A convnet for the 2020s. In *Proceedings of the IEEE/CVF Conference on Computer Vision and Pattern Recognition*, pp. 11976–11986, 2022b.

Jiachen Lu, Jinghan Yao, Junge Zhang, Xiatian Zhu, Hang Xu, Weiguo Gao, Chunjing Xu, Tao Xiang, and Li Zhang. Soft: Softmax-free transformer with linear complexity. *Advances in Neural Information Processing Systems*, 34:21297–21309, 2021.

Xiaofeng Mao, Gege Qi, Yuefeng Chen, Xiaodan Li, Ranjie Duan, Shaokai Ye, Yuan He, and Hui Xue. Towards robust vision transformer. In *Proceedings of the IEEE/CVF conference on Computer Vision and Pattern Recognition*, pp. 12042–12051, 2022.

Sachin Mehta and Mohammad Rastegari. Mobilevit: Light-weight, general-purpose, and mobile-friendly vision transformer. In *International Conference on Learning Representations*.

Niki Parmar, Ashish Vaswani, Jakob Uszkoreit, Lukasz Kaiser, Noam Shazeer, Alexander Ku, and Dustin Tran. Image transformer. In *International conference on machine learning*, pp. 4055–4064. PMLR, 2018.

Hao Peng, Nikolaos Pappas, Dani Yogatama, Roy Schwartz, Noah Smith, and Lingpeng Kong. Random feature attention. In *International Conference on Learning Representations*.

Zhiliang Peng, Wei Huang, Shanzhi Gu, Lingxi Xie, Yaowei Wang, Jianbin Jiao, and Qixiang Ye. Conformer: Local features coupling global representations for visual recognition. In *Proceedings of the IEEE/CVF international conference on computer vision*, pp. 367–376, 2021.

Boris T Polyak and Anatoli B Juditsky. Acceleration of stochastic approximation by averaging. *SIAM journal on control and optimization*, 30(4):838–855, 1992.

Zhen Qin, Weixuan Sun, Hui Deng, Dongxu Li, Yunshen Wei, Baohong Lv, Junjie Yan, Lingpeng Kong, and Yiran Zhong. cosformer: Rethinking softmax in attention. In *International Conference on Learning Representations*.

Ilija Radosavovic, Raj Prateek Kosaraju, Ross B. Girshick, Kaiming He, and Piotr Dollár. Designing network design spaces. In *CVPR*, pp. 10425–10433. Computer Vision Foundation / IEEE, 2020.

Prajit Ramachandran, Niki Parmar, Ashish Vaswani, Irwan Bello, Anselm Levskaya, and Jon Shlens. Stand-alone self-attention in vision models. *Advances in neural information processing systems*, 32, 2019.

Yongming Rao, Wenliang Zhao, Yansong Tang, Jie Zhou, Ser-Nam Lim, and Jiwen Lu. Hornet: Efficient high-order spatial interactions with recursive gated convolutions. In *Advances in Neural Information Processing Systems*.

Pengzhen Ren, Changlin Li, Guangrun Wang, Yun Xiao, Qing Du, Xiaodan Liang, and Xiaojun Chang. Beyond fixation: Dynamic window visual transformer. In *Proceedings of the IEEE/CVF Conference on Computer Vision and Pattern Recognition*, pp. 11987–11997, 2022.

Mark Sandler, Andrew Howard, Menglong Zhu, Andrey Zhmoginov, and Liang-Chieh Chen. Mobilenetv2: Inverted residuals and linear bottlenecks. In *Proceedings of the IEEE conference on computer vision and pattern recognition*, pp. 4510–4520, 2018.

Peter Shaw, Jakob Uszkoreit, and Ashish Vaswani. Self-attention with relative position representations. *arXiv preprint arXiv:1803.02155*, 2018.

Weili Shi and Sheng Li. Improving robustness of vision transformers via data-augmented virtual adversarial training. In *2022 IEEE International Conference on Big Data (Big Data)*, pp. 135–140. IEEE, 2022.

Weili Shi, Ronghang Zhu, and Sheng Li. Pairwise adversarial training for unsupervised class-imbalanced domain adaptation. In *Proceedings of the 28th ACM SIGKDD conference on knowledge discovery and data mining*, pp. 1598–1606, 2022.

Weili Shi, Zhongliang Zhou, Benjamin H Letcher, Nathaniel Hitt, Yoichiro Kanno, Ryo Futamura, Osamu Kishida, Kentaro Morita, and Sheng Li. Aging contrast: A contrastive learning framework for fish re-identification across seasons and years. In *Australasian Joint Conference on Artificial Intelligence*, pp. 252–264. Springer, 2023.

Aravind Srinivas, Tsung-Yi Lin, Niki Parmar, Jonathon Shlens, Pieter Abbeel, and Ashish Vaswani. Bottleneck transformers for visual recognition. In *Proceedings of the IEEE/CVF conference on computer vision and pattern recognition*, pp. 16519–16529, 2021.

Chen Sun, Abhinav Shrivastava, Saurabh Singh, and Abhinav Gupta. Revisiting unreasonable effectiveness of data in deep learning era. In *Proceedings of the IEEE international conference on computer vision*, pp. 843–852, 2017.

Weixuan Sun, Zhen Qin, Hui Deng, Jianyuan Wang, Yi Zhang, Kaihao Zhang, Nick Barnes, Stan Birchfield, Lingpeng Kong, and Yiran Zhong. Vicinity vision transformer. *IEEE Transactions on Pattern Analysis and Machine Intelligence*, 2023.

Mingxing Tan and Quoc Le. Efficientnet: Rethinking model scaling for convolutional neural networks. In *International conference on machine learning*, pp. 6105–6114. PMLR, 2019.

Mingxing Tan and Quoc Le. Efficientnetv2: Smaller models and faster training. In *International conference on machine learning*, pp. 10096–10106. PMLR, 2021.

Rui Tian, Zuxuan Wu, Qi Dai, Han Hu, Yu Qiao, and Yu-Gang Jiang. Resformer: Scaling vits with multi-resolution training. In *Proceedings of the IEEE/CVF Conference on Computer Vision and Pattern Recognition*, pp. 22721–22731, 2023.

Hugo Touvron, Matthieu Cord, Matthijs Douze, Francisco Massa, Alexandre Sablayrolles, and Hervé Jégou. Training data-efficient image transformers & distillation through attention. In *International conference on machine learning*, pp. 10347–10357. PMLR, 2021a.

Hugo Touvron, Matthieu Cord, Alexandre Sablayrolles, Gabriel Synnaeve, and Hervé Jégou. Going deeper with image transformers. In *Proceedings of the IEEE/CVF International Conference on Computer Vision*, pp. 32–42, 2021b.

Hugo Touvron, Matthieu Cord, and Hervé Jégou. Deit iii: Revenge of the vit. In *Computer Vision–ECCV 2022: 17th European Conference, Tel Aviv, Israel, October 23–27, 2022, Proceedings, Part XXIV*, pp. 516–533. Springer, 2022.

Zhengzhong Tu, Hossein Talebi, Han Zhang, Feng Yang, Peyman Milanfar, Alan Bovik, and Yinxiao Li. Maxvit: Multi-axis vision transformer. In *Computer Vision–ECCV 2022: 17th European Conference, Tel Aviv, Israel, October 23–27, 2022, Proceedings, Part XXIV*, pp. 459–479. Springer, 2022.

Ashish Vaswani, Noam Shazeer, Niki Parmar, Jakob Uszkoreit, Llion Jones, Aidan N Gomez, Łukasz Kaiser, and Illia Polosukhin. Attention is all you need. *Advances in neural information processing systems*, 30, 2017.

Huiyu Wang, Yukun Zhu, Bradley Green, Hartwig Adam, Alan Yuille, and Liang-Chieh Chen. Axial-deeplab: Stand-alone axial-attention for panoptic segmentation. In *Computer Vision–ECCV 2020: 16th European Conference, Glasgow, UK, August 23–28, 2020, Proceedings, Part IV*, pp. 108–126. Springer, 2020.

Weihan Wang, Bharat Joshi, Nathaniel Burgdorfer, Konstantinos Batsosc, Alberto Quattrini Lid, Philippos Mordohaia, and Ioannis Rekleitisb. Real-time dense 3d mapping of underwater environments. In *2023 IEEE International Conference on Robotics and Automation (ICRA)*, pp. 5184–5191, 2023a. doi: 10.1109/ICRA48891.2023.10160266.

Weihan Wang, Jiani Li, Yuhang Ming, and Philippos Mordohai. Edi: Eskf-based disjoint initialization for visual-inertial slam systems. In *2023 IEEE/RSJ International Conference on Intelligent Robots and Systems (IROS)*, pp. 1466–1472, 2023b. doi: 10.1109/IROS55552.2023.10342106.

Wenhai Wang, Enze Xie, Xiang Li, Deng-Ping Fan, Kaitao Song, Ding Liang, Tong Lu, Ping Luo, and Ling Shao. Pyramid vision transformer: A versatile backbone for dense prediction without convolutions. In *Proceedings of the IEEE/CVF international conference on computer vision*, pp. 568–578, 2021.

Wenhai Wang, Jifeng Dai, Zhe Chen, Zhenhang Huang, Zhiqi Li, Xizhou Zhu, Xiaowei Hu, Tong Lu, Lewei Lu, Hongsheng Li, et al. Internimage: Exploring large-scale vision foundation models with deformable convolutions. *arXiv preprint arXiv:2211.05778*, 2022a.

Wenhai Wang, Enze Xie, Xiang Li, Deng-Ping Fan, Kaitao Song, Ding Liang, Tong Lu, Ping Luo, and Ling Shao. Pvt v2: Improved baselines with pyramid vision transformer. *Computational Visual Media*, 8(3): 415–424, 2022b.

Wenhai Wang, Jifeng Dai, Zhe Chen, Zhenhang Huang, Zhiqi Li, Xizhou Zhu, Xiaowei Hu, Tong Lu, Lewei Lu, Hongsheng Li, et al. Internimage: Exploring large-scale vision foundation models with deformable convolutions. In *Proceedings of the IEEE/CVF Conference on Computer Vision and Pattern Recognition*, pp. 14408–14419, 2023c.

Xiaolong Wang, Ross Girshick, Abhinav Gupta, and Kaiming He. Non-local neural networks. In *Proceedings of the IEEE conference on computer vision and pattern recognition*, pp. 7794–7803, 2018.

Haiping Wu, Bin Xiao, Noel Codella, Mengchen Liu, Xiyang Dai, Lu Yuan, and Lei Zhang. Cvt: Introducing convolutions to vision transformers. In *Proceedings of the IEEE/CVF International Conference on Computer Vision*, pp. 22–31, 2021.

Zhuofan Xia, Xuran Pan, Shiji Song, Li Erran Li, and Gao Huang. Vision transformer with deformable attention. In *Proceedings of the IEEE/CVF conference on computer vision and pattern recognition*, pp. 4794–4803, 2022.

Tete Xiao, Yingcheng Liu, Bolei Zhou, Yuning Jiang, and Jian Sun. Unified perceptual parsing for scene understanding. In *Proceedings of the European conference on computer vision (ECCV)*, pp. 418–434, 2018.

Tete Xiao, Mannat Singh, Eric Mintun, Trevor Darrell, Piotr Dollár, and Ross Girshick. Early convolutions help transformers see better. *Advances in Neural Information Processing Systems*, 34:30392–30400, 2021.

Enze Xie, Wenhai Wang, Zhiding Yu, Anima Anandkumar, Jose M Alvarez, and Ping Luo. Segformer: Simple and efficient design for semantic segmentation with transformers. *Advances in Neural Information Processing Systems*, 34:12077–12090, 2021.

Saining Xie, Ross Girshick, Piotr Dollar, Zhuowen Tu, and Kaiming He. Aggregated residual transformations for deep neural networks. In *Proceedings of the IEEE Conference on Computer Vision and Pattern Recognition (CVPR)*, July 2017.

Jianwei Yang, Chunyuan Li, Pengchuan Zhang, Xiyang Dai, Bin Xiao, Lu Yuan, and Jianfeng Gao. Focal attention for long-range interactions in vision transformers. In *NeurIPS*, pp. 30008–30022, 2021.

Kun Yuan, Shaopeng Guo, Ziwei Liu, Aojun Zhou, Fengwei Yu, and Wei Wu. Incorporating convolution designs into visual transformers. In *Proceedings of the IEEE/CVF International Conference on Computer Vision*, pp. 579–588, 2021.

Hao Zhang, Feng Li, Shilong Liu, Lei Zhang, Hang Su, Jun Zhu, Lionel Ni, and Harry Shum. Dino: Detr with improved denoising anchor boxes for end-to-end object detection. In *International Conference on Learning Representations*, 2022a.

Pengchuan Zhang, Xiyang Dai, Jianwei Yang, Bin Xiao, Lu Yuan, Lei Zhang, and Jianfeng Gao. Multi-scale vision longformer: A new vision transformer for high-resolution image encoding. In *Proceedings of the IEEE/CVF international conference on computer vision*, pp. 2998–3008, 2021.

Xiaosong Zhang, Yunjie Tian, Lingxi Xie, Wei Huang, Qi Dai, Qixiang Ye, and Qi Tian. Hivit: A simpler and more efficient design of hierarchical vision transformer. In *The Eleventh International Conference on Learning Representations*, 2022b.

Hengshuang Zhao, Jiaya Jia, and Vladlen Koltun. Exploring self-attention for image recognition. In *Proceedings of the IEEE/CVF conference on computer vision and pattern recognition*, pp. 10076–10085, 2020.

Sixiao Zheng, Jiachen Lu, Hengshuang Zhao, Xiatian Zhu, Zekun Luo, Yabiao Wang, Yanwei Fu, Jianfeng Feng, Tao Xiang, Philip HS Torr, et al. Rethinking semantic segmentation from a sequence-to-sequence perspective with transformers. In *Proceedings of the IEEE/CVF conference on computer vision and pattern recognition*, pp. 6881–6890, 2021.

Bolei Zhou, Hang Zhao, Xavier Puig, Sanja Fidler, Adela Barriuso, and Antonio Torralba. Scene parsing through ade20k dataset. In *Proceedings of the IEEE Conference on Computer Vision and Pattern Recognition*, pp. 633–641, 2017.

Daquan Zhou, Zhiding Yu, Enze Xie, Chaowei Xiao, Animashree Anandkumar, Jiashi Feng, and Jose M Alvarez. Understanding the robustness in vision transformers. In *International Conference on Machine Learning*, pp. 27378–27394. PMLR, 2022a.

Zhongliang Zhou, Nathaniel P Hitt, Benjamin H Letcher, Weili Shi, and Sheng Li. Pigmentation-based visual learning for salvelinus fontinalis individual re-identification. In *2022 IEEE International Conference on Big Data (Big Data)*, pp. 6850–6852. IEEE, 2022b.

A Appendix

A.1 Theoretical Analysis

The proof of Proposition 1 is provided below.

Proof 1 *Assume $\theta_0 \leq \theta_1 \leq ... \leq \theta_{J-1}$ for angles between the target query and all the keys. J is the total number of the tokens. V is the value vector. According to our angular self-attention, the embedding of target*

Table 13: Object detection and instance segmentation performance of our model and the baseline models with Mask R-CNN framework with 1x schedule training scheme. The FLOPs are measured at resolution 800 × 1280. [cos] and [quad] denote cosine and quadratic function, respectively.

Backbone	#Param(M)	#FLOPs(G)	AP^b	AP^b_{50}	AP^b_{75}	AP^m	AP^m_{50}	AP^m_{75}
ResNet-50 (He et al., 2016)	44	260	38.0	58.6	41.4	34.4	55.1	36.7
PVT-S (Wang et al., 2021)	44	245	40.4	62.9	43.8	37.8	60.1	40.3
ViL-S (Zhang et al., 2021)	45	218	44.9	67.1	49.3	41.0	64.2	44.1
TwinsP-S (Chu et al., 2021a)	44	245	42.9	65.8	47.1	40.0	62.7	42.9
Twins-S (Chu et al., 2021a)	44	228	43.4	66.0	47.3	40.3	63.2	43.4
Swin-T (Liu et al., 2021)	48	264	42.2	64.6	46.2	39.1	61.6	42.0
DAT-T (Xia et al., 2022)	48	272	44.4	67.6	48.5	40.4	64.2	43.1
CSWin-T (Dong et al., 2022)	42	279	**46.7**	68.6	**51.3**	**42.2**	65.6	45.4
DWAViT-T[cos] (Ours)	42	255	46.2	69.2	50.8	41.7	65.9	44.7
DWAViT-T[quad] (Ours)	42	255	46.6	**69.6**	**51.3**	**42.2**	**66.3**	**45.7**
Res101 (He et al., 2016)	63	336	40.4	61.1	44.2	36.4	57.7	38.8
PVT-M (Wang et al., 2021)	64	302	42.0	64.4	45.6	39.0	61.6	42.1
ViL-M (Zhang et al., 2021)	60	261	44.6	66.3	48.5	40.7	63.8	43.7
TwinsP-B (Chu et al., 2021a)	64	302	44.6	66.7	48.9	40.9	63.8	44.2
Twins-B (Chu et al., 2021a)	76	340	45.2	67.6	49.3	41.5	64.5	44.8
Swin-S (Liu et al., 2021)	69	354	44.8	66.6	48.9	40.9	63.4	44.2
CSWin-S (Dong et al., 2022)	54	342	47.9	70.1	52.6	43.2	67.1	46.2
DAT-S (Xia et al., 2022)	69	378	47.1	69.9	51.5	42.5	66.7	45.4
DWAViT-S[cos] (Ours)	64	338	48.0	70.7	52.6	**43.3**	67.6	46.5
DWAViT-S[quad] (Ours)	64	338	**48.2**	70.8	52.8	**43.3**	**67.7**	**46.6**
X101-64 (Xie et al., 2017)	101	493	42.8	63.8	47.3	38.4	60.6	41.3
PVT-L (Wang et al., 2021)	81	364	42.9	65.0	46.6	39.5	61.9	42.5
CSWin-B (Dong et al., 2022)	97	526	**48.7**	70.4	**53.9**	**43.9**	67.8	**47.3**
DWAViT-B[cos] (Ours)	97	462	48.6	71.1	53,7	43.6	**68.0**	46.9
DWAViT-B[quad] (Ours)	97	462	48.6	**71.2**	53.6	43.6	67.9	47.1

tokens can be expressed as:

$$
\begin{aligned}
\mathcal{O} &= \frac{1}{C}\sum_j \exp(s(\theta_j)/\tau)V_j \\
&= \frac{1}{C}\exp(\frac{s(\theta_0)}{\tau})(V_0 + \exp(\frac{s(\theta_1)-s(\theta_0)}{\tau})V_1 + ... \\
&+ \exp(\frac{s(\theta_{J-1})-s(\theta_0)}{\tau})V_{J-1}) \\
&= \frac{1}{C}\exp(\frac{s(\theta_0)}{\tau})(V_0 + \omega_1 V_1 + ... + \omega_{J-1}V_{J-1}), \\
&\propto V_0 + \omega_1 V_1 + \cdots + \omega_{J-1}V_{J-1},
\end{aligned}
\tag{7}
$$

where $\omega_j = \exp(\frac{s(\theta_j)-s(\theta_0)}{\tau})$ and C is normalization coefficient. Since $\theta_j > \theta_0$ and $s(\theta_j) < s(\theta_0)$, $\omega_j \in (0,1)$.

A.2 Experiment

The results on object detection and instance segmentation of our model and the baseline models with Mask R-CNN (He et al., 2017) framework with 1× schedule are illustrated in Table 13. The baseline methods include the latest ViT models such as CSwin (Dong et al., 2022) and DAT (Xia et al., 2022). Specifically, Swin Transformer (Liu et al., 2021), DAT (Xia et al., 2022) and CSwin (Dong et al., 2022) are baselines for exact comparison. These baselines and our method adopt MMDetection toolbox (Chen et al., 2019) to perform the experiment and use models pre-trained on ImageNet-1K only as the feature extractor. For tiny-sized models the experimental results show that the DWAViT-T can achieve on par or better result against that of CSWin (Dong et al., 2022). For instance, the AP^b_{50} of DWAViT-T(quad) can achieve 69.6%, which is 1.0% higher than that of CSWin (Dong et al., 2022). And the AP^m of DWAViT-T(quad) is 42.2%,

Table 14: Object detection and instance segmentation performance of our model and the baseline models with Cascade Mask R-CNN framework. The model is trained with a 3x scheme. The FLOPs are measured at resolution 800×1280. [cos] and [quad] denote cosine and quadratic function, respectively.

Backbone	#Param(M)	#FLOPs(G)	AP^b	AP^b_{50}	AP^b_{75}	AP^m	AP^m_{50}	AP^m_{75}
Res50 (He et al., 2016)	82	739	46.3	64.3	50.5	40.1	61.7	43.4
Swin-T (Liu et al., 2021)	86	745	50.5	69.3	54.9	43.7	66.6	47.1
DAT-T (Xia et al., 2022)	86	750	51.3	70.1	55.8	44.5	67.5	48.1
NAT-T (Hassani et al., 2023)	85	737	51.4	70.0	55.9	44.5	67.6	47.9
GC ViT-T (Hatamizadeh et al., 2023)	85	770	51.6	70.4	56.1	44.6	67.8	48.3
DWAViT-T[cos] (Ours)	80	734	**52.2**	**71.0**	**57.0**	**45.1**	68.3	**49.0**
DWAViT-T[quad] (Ours)	80	734	51.0	70.6	56.7	44.9	**68.5**	48.8
X101-32 (Xie et al., 2017)	101	819	48.1	66.5	52.4	41.6	63.9	45.2
Swin-S (Liu et al., 2021)	107	838	51.8	70.4	56.3	44.7	67.9	48.5
DAT-S (Xia et al., 2022)	107	807	**52.7**	**71.7**	**57.2**	45.5	**69.1**	49.3
NAT-S (Hassani et al., 2023)	108	809	52.0	70.4	56.3	44.9	68.1	48.6
GC ViT-S (Hatamizadeh et al., 2023)	108	866	52.4	71.0	57.1	45.4	68.5	49.3
DWAViT-S[cos] (Ours)	102	817	52.5	71.3	57.0	**45.6**	68.9	49.6
DWAViT-S[quad] (Ours)	102	817	52.5	71.4	**57.2**	**45.6**	68.9	**49.9**
X101-64 (Xie et al., 2017)	140	972	48.3	66.4	52.3	41.7	64.0	45.1
Swin-B (Liu et al., 2021)	145	982	51.9	70.9	56.5	45.0	68.4	48.7
NAT-B (Hassani et al., 2023)	147	931	52.5	71.1	57.1	45.2	68.6	49.0
GC ViT-B (Hatamizadeh et al., 2023)	146	1018	**52.9**	**71.7**	**57.8**	**45.8**	**69.2**	**49.8**
DWAViT-B[cos] (Ours)	134	940	52.5	71.3	57.0	45.6	69.0	49.6
DWAViT-B[quad] (Ours)	134	940	52.8	71.6	57.3	45.7	69.1	49.5

which is on par with that of CSWin (Dong et al., 2022). The DWAViT-S with quadratic self-attention can outperform all the baseline methods on all the metrics. The AP^b and AP^m can reach 48.2% and 43.3%, respectively. Furthermore, DWAViT-B can achieve best results on AP^b_{50} and AP^m_{50}.

Table 14 show the performance of our model and the baseline models with Cascade Mask R-CNN (Cai & Vasconcelos, 2018) framework on object detection and instance segmentation. Swin Transformer (Liu et al., 2021) and DAT (Xia et al., 2022) are the major baselines for the exact comparison. The experimental results show that our DWAViT outperforms baseline methods. DWAViT-T can achieve 52.2% on AP^b and 45.1% on AP^m, and DWAViT-S can achieves 52.5% on AP^b and 45.6% on AP^m. The DWAViT-S with quadratic self-attention can achieve 45.6% and 49.9% on AP^m and AP^m_{75}, respectively, which is 0.1% and 0.3% higher than that of DAT-S (Xia et al., 2022).

The performance of DWAViT-S and DWAViT-B on semantic segmentation task are illustrated in Table 15. The baseline models include XCiT (Ali et al., 2021), Swin Transformer (Liu et al., 2021), DaViT (Ding et al., 2022), Focal Transformer (Yang et al., 2021) and DAT (Xia et al., 2022). The experimental results suggest that our DWAViT with cosine self-attention can achieve the best performance and the mIoU can reach 49.3% and 49.8% for DWAViT-S and DWAViT-B, respectively.

A.3   Ablation Study

In the ablation study we first compare the performance of our model with traditional scaled dot-product self-attention and our proposed angular self-attention and evaluate the performance on ImageNet-1K classification, COCO object detection and ADE20K semantic segmentation. We adopt the DWAViT-T as the backbone in three tasks. In object detection, Mask R-CNN is adopted as the framework and the model is trained with 36 epochs. In semantic segmentation Upernet is adopted as the framework and the model is trained with 160K iteration. The performance of model on semantic segmentation are illustrated in Table 16. The performance of our model with scaled dot-product self-attention is lower than that of our model with the proposed angular self-attention. On some tasks the gap of the performance is more obvious. For instance, on semantic segmentation our model of scaled dot-product self-attention only achieves 44.7% on mIoU, approximately 3% lower than that of our model with cosine self-attention. The experimental results suggest our angular self-attention can model the relationship of the tokens successfully and the angular self-attention is a powerful alternative to the traditional scaled dot-product self-attention.

Table 15: The semantic segmentation performance of DWAViT-S, DWAViT-B and baselines on ADE20K. The FLOPs are calculated with resolution 512×2048. [cos] and [quad] denote cosine and quadratic function, respectively.

Backbone	#Param(M)	#FLOPs(G)	mIoU
ResNet-101 (He et al., 2016)	86	1029	44.9
XCiT-S24/16 (Ali et al., 2021)	76	1053	46.9
TwinsP-B (Chu et al., 2021a)	74	977	47.1
XCiT-M24/16 (Ali et al., 2021)	112	1213	47.6
Swin-S (Liu et al., 2021)	81	1038	47.6
Twins-B (Chu et al., 2021a)	89	1020	47.7
Focal-S (Yang et al., 2021)	85	1130	48.0
DaViT-T (Ding et al., 2022)	81	1030	48.8
DAT-T (Xia et al., 2022)	83	1079	48.3
GC ViT-S (Hatamizadeh et al., 2023)	84	1163	48.3
NAT-S (Hassani et al., 2023)	82	1010	48.0
DWAViT-S[cos] (Ours)	75	1015	**49.3**
DWAViT-S[quad] (Ours)	75	1015	47.8
XCiT-M24/8 (Ali et al., 2021)	110	2161	48.4
Swin-B (Liu et al., 2021)	121	1841	48.1
Focal-B (Yang et al., 2021)	126	1354	49.0
DaViT-B (Ding et al., 2022)	121	1175	49.4
DAT-B (Xia et al., 2022)	121	1212	49.4
GC ViT-B (Hatamizadeh et al., 2023)	125	1348	49.2
NAT-B (Hassani et al., 2023)	123	1137	48.5
DWAViT-B[cos] (Ours)	108	1143	**49.8**
DWAViT-B[quad] (Ours)	108	1143	49.1

Table 16: The performance of our proposed DWAViT with angular self-attention, scaled dot-product self-attention and linearized self-attention on the semantic segmentation. FLOPs are calculated with resolution 512×2048. The [dot product], [cos] and [quad] in the square bracket denote scaled dot-product, cosine and quadratic function, respectively.

Backbone	Param(M)	FLOPs(G)	mIoU
DWAViT-T[dot product]	52	930	44.7
DWAViT-T[linear]	52	930	44.1
DWAViT-T[cos] (Ours)	52	930	**47.5**
DWAViT-T[quad] (Ours)	52	930	45.4

We also compare the performance of our model with the proposed dual local window with the shifted window proposed by Swin Transformer (Liu et al., 2021). In the experiment we replace the dual local window with the shifted local window and evaluate the performance of the model on ImageNet-1K classification, COCO object detection and ADE20K semantic segmentation. We adopt the DWAViT-T(quad) as the backbone in three tasks. The results on ADE20K semantic segmentation are illustrated in Table 17, respectively. On semantic segmentation, our model with shifted local window can achieve better performance than that of our model with dual local window. However, on the object detection task, the performance of our model with shifted window is lower to that of our model with dual local window on all metrics. To wrap up, our dual local window is effective in the modeling of the relationship of tokens and it can achieve better performance than that of the shifted local window on some tasks.

Table 17: The performance of our proposed DWAViT with the dual local window and shifted local window on the semantic segmentation. We adopt the quadratic self-attention and the FLOPs are calculated with resolution 512×2048.

Backbone	Param(M)	FLOPs(G)	mIoU
DWAViT-T[shifted window]	52	933	46.2
DWAViT-T[dual window] (Ours)	52	930	45.4